Bioorganic & Medicinal Chemistry xxx (xxxx) xxxx

Contents lists available at ScienceDirect

Bioorganic & Medicinal Chemistry

journal homepage: www.elsevier.com/locate/bmc

Design, synthesis and evaluation of structurally diverse chrysin-chromene-spirooxindole hybrids as anticancer agents

Wen-Hui Zhang[a], Shuang Chen[a], Xiong-Li Liu[a,*], Ting-Ting Feng[b], Wu-De Yang[b], Ying Zhou[b,*]

[a] Guizhou Medicine Edible Plant Resources Research and Development Center, Guizhou University, Guiyang 550025, China
[b] College of Pharmaceutical Sciences, Guizhou University of Traditional Chinese Medicine, Guiyang 550025, China

ARTICLE INFO

Keywords:
Chrysin
Spirooxindole
Chromene
Hybrids
Anticancer agents

ABSTRACT

A series of structurally diverse chrysin-chromene-spirooxindole hybrids were designed, synthesized *via* a Knoevenagel/Michael/cyclization of chrysin and isatylidene malononitrile derivatives through utilizing a hybrid pharmacophore approach. The newly synthesized compounds were evaluated for their *in vitro* anticancer activity, and most of the compounds showed stronger anti-proliferative activity than parent compound chrysin. In particular, compound **3e** had the highest cytotoxicity towards A549 cells (IC_{50} = 3.15 ± 0.51 μM), and had better selectivity in A549 cells and normal MRC-5 cells. Furthermore, compound **3e** could significantly inhibit the proliferation and migration of A549 cells in a dose-dependent manner, as well as induce the apoptosis possibly through mitochondria-mediated caspase-3/8/9 activation and multi-target co-regulation of the p53 signaling pathway. Thus, our results provide *in vitro* evidence that compound **3e** may be a potential candidate for the development of new anti-tumour drugs.

1. Introduction

Molecular hybridization is a valuable useful approach that comprises the incorporation of two or more pharmacophoric moieties of different bioactive substances into a single entity.[1] This structural derivatization strategy can result in hybrid molecules acting through the same mechanism of action or different mechanisms of action.[1,2] In the last few years, molecular hybridization strategy has emerged as a prime strategy for the discovery of innovative anticancer drugs that can potentially overcome some drawbacks of the conventional anticancer drugs.

Flavonoids, as the privileged molecular scaffolds in drug discovery, which are one of the most representative classes of plant secondary metabolites, have attracted the scientific interest because they display a remarkable spectrum of biological activities, including important chemopreventive and chemotherapeutic effects on cancer.[3–8] It is important to know that flavonoids are generally safe and without adverse effects and that many flavonoids occur in our diet. As a natural flavone, chrysin[9–14] has also been reported to exhibit anticancer activities. However, few chrysin derivatives and their biological activities have been reported by the modification at C-7 of A-ring.[15–17] Based on the above considerations, we proposed that incorporating two or more pharmacophoric groups into the chrysin structure might be an effective strategy for discovering novel chrysin-derivated hybrids with potential bioactivity (Fig. 1).

Chromene, as one of the privileged motif, has widely appeared in natural products and drug molecules.[18] Moreover, in recent years chromene-derivated hybrids have played an ever-increasing role in the field of medicinal chemistry.[19–21] For example, in the case of cancer therapy, the tumour antagonist HA14–1 is a new functionalized compound that induce apoptosis or programmed cell death in follicular lymphoma B cells and leukemia HL-60 cells.[22] The 2-amino-3-cyano-4H-chromene MX58151 is a promising class of proapoptotic small-molecule agent with multiple action modes against the lung cancer cell line H1299, the breast cancer cell line T47D, and the colorectal cancer cell line DLD-1 (Fig. 1).[23,24]

Spirooxindoles[25–31] are an inportant class of scaffolds found in many natural products and drug cancidate molecules (such as CFI-400945, SAR405838, *etc.*). CFI-400945 is a polo-like kinase 4 inhibitor, as a potential anticancer agent,[30] and SAR405838 is an optimized inhibitor of MDM2-p53 interaction that induces complete and durable tumour regression.[31] This is especially true for the last few years which have seen a phenomenal increase in the number of reports on the construction of structurally diverse spirooxindoles, which may in part be due to the increasing recognition of their biological significance. However, to the best of our knowledge, there have been no reports for the synthesis of spirooxindole derivatives containing flavonoid moiety (Fig. 1).

* Corresponding authors.
E-mail addresses: xlliu1@gzu.edu.cn (X.-L. Liu), yzhou@gzu.edu.cn (Y. Zhou).

https://doi.org/10.1016/j.bmc.2019.115109
Received 22 June 2019; Received in revised form 4 September 2019; Accepted 11 September 2019

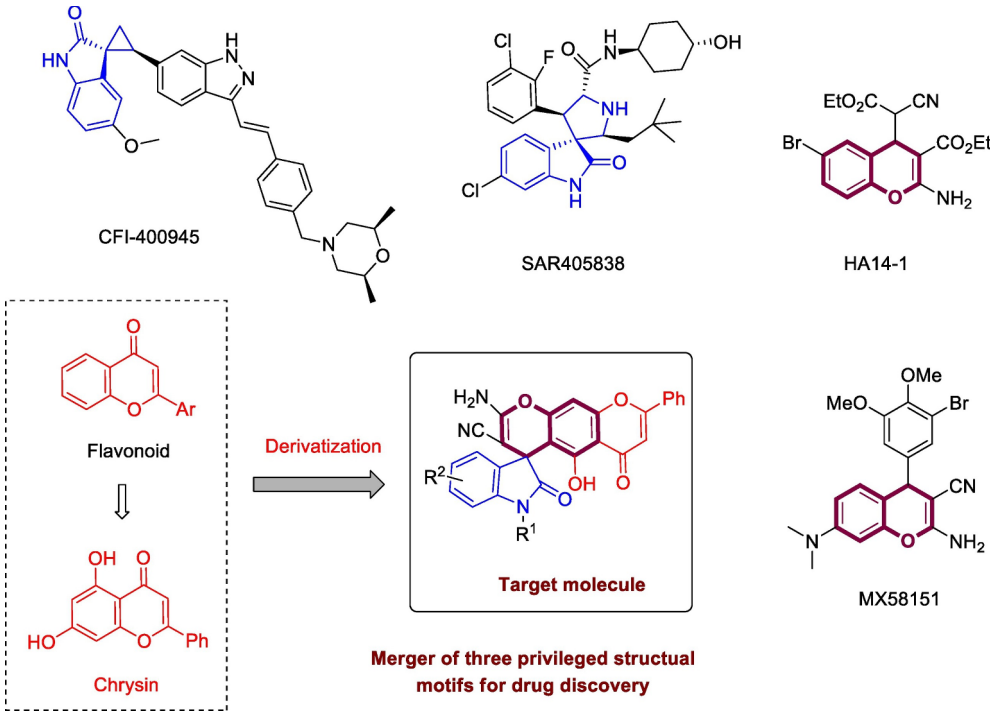

Fig. 1. Representative anticancer agents and our target molecule.

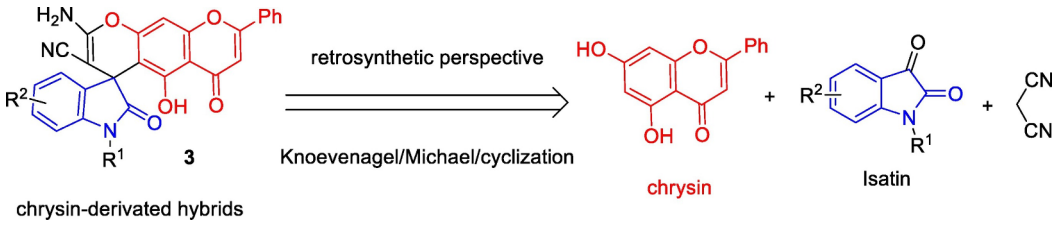

Scheme 1. Our strategy for construction of chrysin-chromene-spirooxindole hybrids.

Over the last decade, numerous studies pointed out the importance of spirooxindole-based anticancer hybrids as promising chemotherapeutic agents. Several research groups adopted molecular hybridization approach for the design of spirooxindole-derivated hybrids as potent anti-proliferative agents.[32–35] Considering the wide occurrence of chromenes and flavonoids in natural products and drugs, herein, with the prime aim of developing potent anticancer agents, we hypothesized that the structurally diverse chrysin-chromene-spirooxindole hybrids could be constructed *via* a Knoevenagel/Michael/cyclization of chrysin, isatins and malononitrile. To the best of our knowledge, if successful, this is the first example of chrysin-fused spirooxindoles, and is also the first example of flavonoid-fused spirooxindoles (Scheme 1).

2. Results and discussion

2.1. Chemistry

Preparation of the chrysin-chromene-spirooxindole hybrids (**3a-z**) was achieved *via* a Knoevenagel/Michael/cyclization of chrysins **1**, isatins **2** and malononitrile in methanol in the presence of 1.5 eq of Ca $(OH)_2$ in 70–87% yields (for details, reaction optimization experiments see the SI). It is important to mention that the electronic nature of the substituents on the oxindole core of isatins **2** had some impact on the yields of the products. As indicated in Scheme 2, isatins **2** containing electronwithdrawing groups provided higher yields than their electron-donating counterparts. The reactions were also shown to work well with a range of chrysins **1** bearing either electronwithdrawing or electron-donating groups in the C-ring to give the desired products **3v-z** with very good yields (70–86%).

All the target hybrids **3** were deduced from spectroscopic studies (^{1}H NMR, ^{13}C NMR and EI-HRMS), and were determined through single-crystal X-ray analysis of compounds **3c** (Fig. 2).[36]

The plausible mechanism for the formation of compounds (**3a-z**) is shown in Scheme 3 which involved three steps. The initial step is assumed to be the Knoevenagel condensation between the isatin **2** and malononitrile to form isatylidene malononitrile intermediate *in situ*. In the next step, the intermediate undergoes Michael-type addition with chrysin **1** followed by an intramolecular cyclization to give target chrysin-chromene-spirooxindole hybrids **3**.

2.2. In vitro biological studies

2.2.1. MTT assay

Compounds **3a-z** were evaluated for *in vitro* anticancer activities towards human lung cancer cell lines (A549 and H1299), human leukemic cell line (K562) and prostate cancer cell line (PC-3) by the MTT assay with the parent compound chrysin as a positive control. Besides, commercially available broad-spectrum anticancer drug cisplatin also was used as the reference drug.[37] As shown in Table 1, the newly synthesized compounds were evaluated for their *in vitro* anticancer activity, and some of the compounds showed stronger anti-proliferative activity against A549, H1299, K562 and PC-3 than parent compound chrysin, and demonstrated equipotent potency compared with the reference drug of cisplatin.

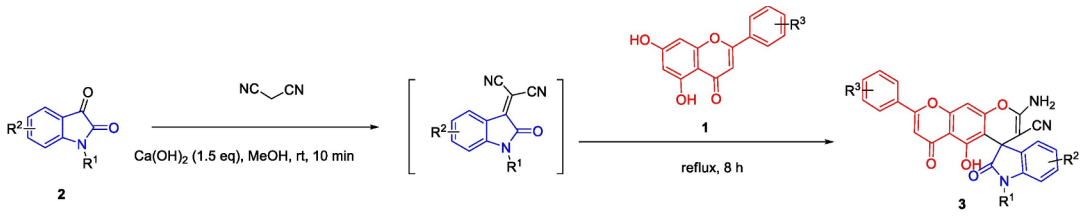

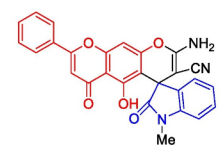
3a: 72%

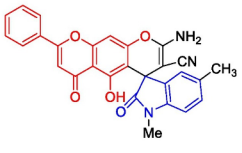
3b: 71%

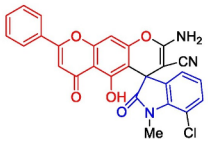
3c: 86%

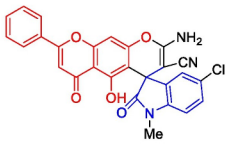
3d: 84%

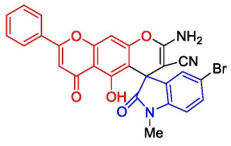
3e: 87%

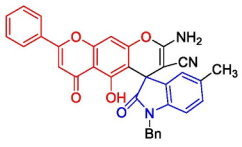
3f: 78%

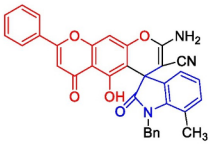
3g: 75%

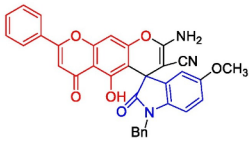
3h: 71%

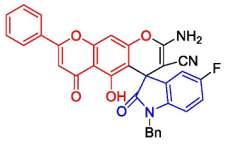
3i: 85%

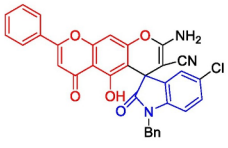
3j: 86%

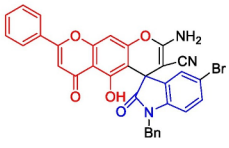
3k: 84%

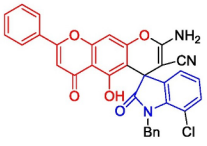
3l: 85%

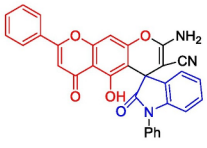
3m: 81%

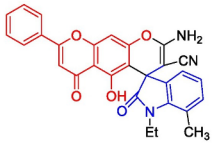
3n: 73%

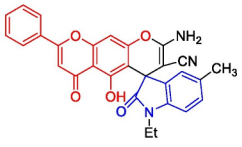
3o: 75%

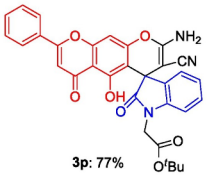
3p: 77%

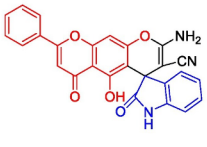
3q: 74%

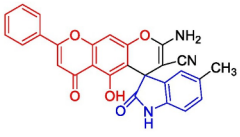
3r: 70%

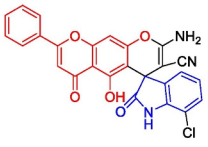
3s: 77%

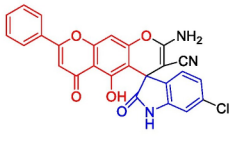
3t: 76%

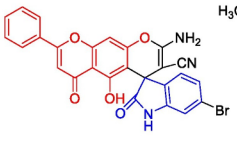
3u: 75%

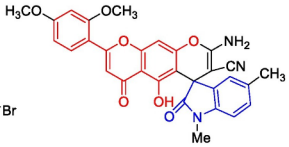
3v: 70%

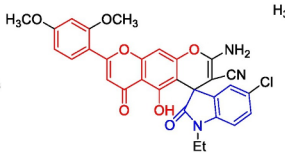
3w: 85%

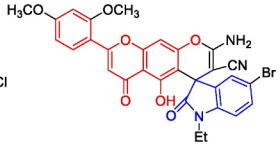
3x: 86%

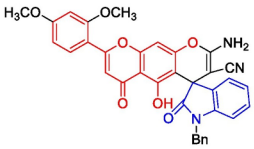
3y: 73%

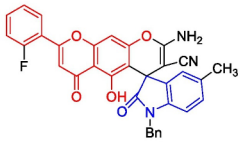
3z: 71%

Scheme 2. Substrate scope to chrysin-chromene-spirooxindole hybrids. Reagents and conditions: a mixture of isatin **2** (0.8 mmol), malononitrile (1.0 mmol) and $Ca(OH)_2$ (0.8 mmol, 59.2 mg) in 5.0 mL of methanol was stirred at room temperature for 10 min followed by the addition of chrysin **1** (0.5 mmol), which was stirred under reflux for 8 h.

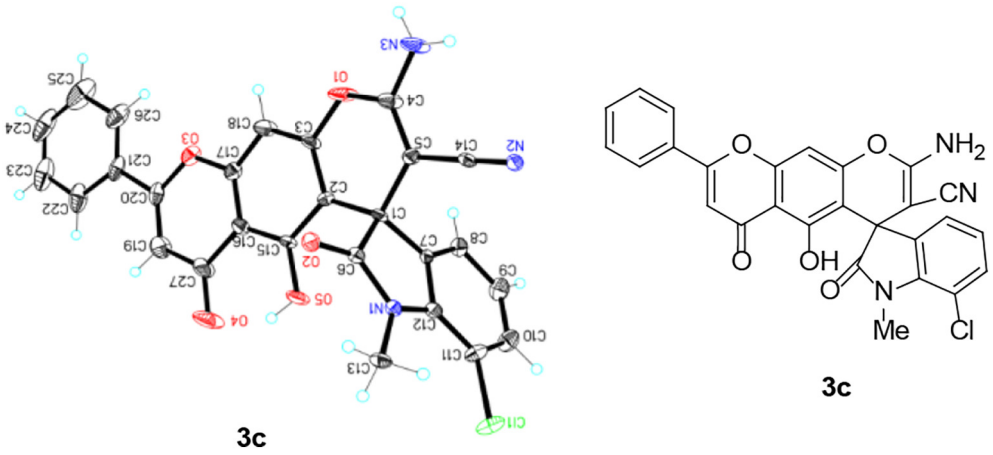

Fig. 2. X-ray crystallographic structure of **3c**.

The MTT assay demonstrated that compounds **3v-x** were equipotent with cisplatin towards K562 (IC_{50} < 20.00 μM). Compounds **3b**, **3d**, **3e**, **3t** and **3u** exhibited the highest anti-proliferative activity against both A549 and K562 (IC_{50} < 10.00 μM). Due to the low solubility of some of these compounds in RPMI-1640 medium, a general structure-activity relationship to anticancer effect could not be summarized from only 26 compounds, the following points were noteworthy: (1) a chromene-spirooxindole moiety located in the chrysin skeleton is beneficial for the activity, and (2) a halogen atom substituent in the isatin improves the potency, especially for K562.

Gratifyingly, the results in Table 1 demonstrated that 5-brom-substituted derivative **3e** showed the strongest cytotoxicity against A549 cells. Therefore, we tested the cytotoxicity of compound **3e** against normal lung fibroblast MRC-5. As shown in Table 2, it showed only slight cytotoxicity towards normal lung fibroblast MRC-5. The results demonstrate that compound **3e** has good selectivity between A549 cells and normal lung fibroblast MRC-5. Thus, compound **3e** was taken forward to further explore its possible cytotoxicity mechanism in A549 cells.

2.2.2. *Anti-proliferative effects of compound **3e** on colony formation in A549 cells*

Anchorage-independent cell growth, which is a key aspect of the tumour phenotype, has been connected with tumour cell aggressiveness *in vivo*.[38] Therefore, clone and soft agar assays were used to confirm the effect of compound **3e** on the colony formation ability of A549 cells.[39,40] As shown in Fig. 3, compared with the control, as the concentration of compound **3e** increased, the size of the colonies formed by the A549 cells decreased, and the number of colonies became fewer. These results indicate that compound **3e** significantly inhibited the anchorage-independent growth of A549 cells *in vitro*.

2.2.3. *Compound **3e** treatment induces apoptosis in A549 cells*

To investigate whether compound **3e** could induce apoptosis of A549 cells, we first observed the morphological changes of A549 cells after compound **3e** treatment for 24 h. As shown in Fig. 4A, as the concentration of compound **3e** increased, the cells began to round, and the adhesion became poor. Second, AO-EB double staining (Fig. 4B) showed chromatin shrinkage, and apoptotic bodies occurred at especially high concentrations. Finally, PI single staining (Fig. 4C) was used to confirm the morphological changes associated with apoptosis in A549 cells, including cell membrane boundaries becoming compromised and presenting fragments of varying sizes. Thus, compound **3e** treatment altered the morphology of A549 cells.

Based on the above results, the most important feature of apoptosis is DNA damage.[41] Therefore, we examined apoptosis in compound **3e**-treated A549 cells *via* the formation of a DNA ladder. As shown in Fig. 4D, the DNA ladder became increasingly apparent as the compound concentration increased. Next, the effect of compound **3e** treatment on apoptosis in A549 cells was confirmed by flow cytometry. The results are shown in Fig. 4E. The percentage of apoptosis in A549 cells gradually increased, especially at high concentrations. Thus, these results suggest that compound **3e** treatment induces apoptosis of A549 cells in a dose-dependent manner.

2.2.4. *Effect of compound **3e** on ROS production in A549 cells*

Studies early have demonstrated that overproduction of intracellular ROS tended to attack DNA and cause DNA strand break

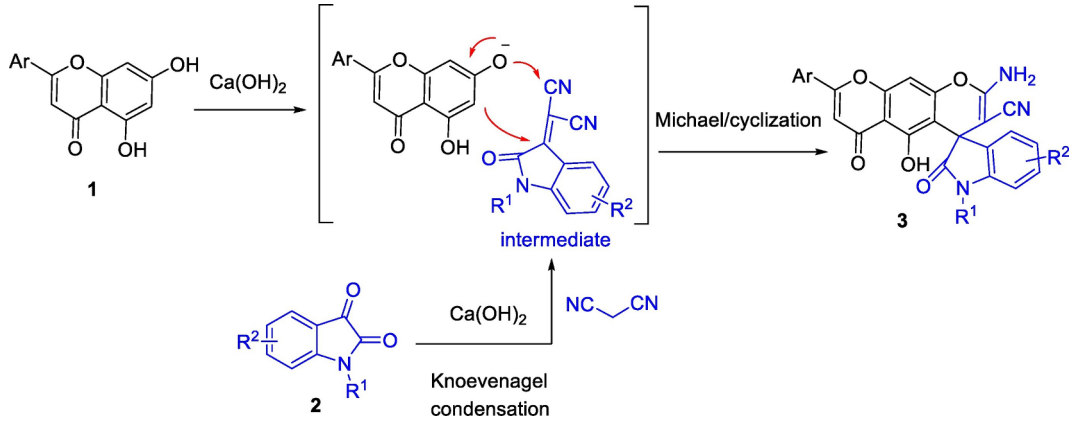

Scheme 3. A plausible reaction mechanism.

Table 1
In vitro cytotoxic activity of the twenty compounds **3a-t** towards K562, A549, H1299 and PC-3 cells.

Compound	IC_{50} (μM)[a]			
	A549	K562	H1299	PC-3
3a	> 50.00	> 50.00	> 50.00	> 50.00
3b	7.06 ± 0.82	5.87 ± 0.94	10.18 ± 1.11	> 50.00
3c	> 50.00	41.40 ± 1.31	> 50.00	> 50.00
3d	4.72 ± 0.35	4.34 ± 0.62	11.18 ± 0.92	21.43 ± 0.98
3e	3.15 ± 0.51	4.10 ± 1.24	7.61 ± 0.63	20.28 ± 1.45
3f	> 50.00	> 50.00	> 50.00	> 50.00
3g	> 50.00	> 50.00	> 50.00	> 50.00
3h	> 50.00	> 50.00	> 50.00	> 50.00
3i	> 50.00	> 50.00	> 50.00	> 50.00
3j	> 50.00	36.32 ± 1.50	> 50.00	> 50.00
3k	> 50.00	36.40 ± 1.22	> 50.00	> 50.00
3l	> 50.00	47.84 ± 1.35	> 50.00	> 50.00
3m	> 50.00	> 50.00	> 50.00	> 50.00
3n	> 50.00	> 50.00	> 50.00	> 50.00
3o	> 50.00	> 50.00	> 50.00	> 50.00
3p	> 50.00	> 50.00	> 50.00	> 50.00
3q	37.62	36.41	> 50.00	> 50.00
3r	> 50.00	> 50.00	> 50.00	> 50.00
3s	> 50.00	37.47	> 50.00	> 50.00
3t	8.47	9.25	16.61	25.69
3u	9.34	8.70	14.38	24.77
3v	> 50.00	12.15 ± 1.07	> 50.00	> 50.00
3w	> 50.00	8.45 ± 0.75	> 50.00	> 50.00
3x	> 50.00	16.12 ± 0.81	> 50.00	> 50.00
3y	> 50.00	> 50.00	> 50.00	> 50.00
3z	> 50.00	> 50.00	> 50.00	> 50.00
Chrysin[b]	> 50.00	> 50.00	> 50.00	> 50.00
DDP[c]	17.58 ± 1.12	12.17 ± 0.84	15.24 ± 1.04	19.15 ± 1.28

[a] IC_{50}: The concentration which results in 50% of tumour cell proliferation inhibition after 48 h of compounds treatment. Data were represented as means ± SD obtained in at least three independent experiments.
[b] Parent compound chrysin used as a positive control.
[c] DDP (cisplatin) used as the reference drug.

Table 2
In vitro cytotoxic activity of the compound **3e** towards normal cells MRC-5.

Compound	IC_{50} (μM)[a]	
	A549	MRC-5
3e	3.15 ± 0.51	> 100.00
Chrysin[b]	> 50.00	> 100.00
DDP[c]	16.58 ± 1.12	> 100.00

[a] IC_{50}: The concentration which results in 50% of tumour cell proliferation inhibition after 48 h of compounds treatment. Data were represented as means ± SD obtained in at least three independent experiments.
[b] Parent compound chrysin used as a positive control.
[c] DDP (cisplatin) used as the reference drug.

leading to cell apoptosis.[42] Therefore, we examined the level of intracellular ROS in A549 cells treated with compound **3e** at different concentrations for 24 h by using a fluorescent probe DCFH-DA. As shown in Fig. 5, there was no bright fluorescence image in the control group, while brighter fluorescent images were detected as the concentration was changed, especially at high concentrations. These results demonstrate that compound **3e** could increase the production of intracellular ROS in a dose-dependent manner.

2.2.5. Activation of caspase in A549 cells after compound *3e* treatment

The caspase family plays an important role in the process of apoptosis.[36] Therefore, we examined the activities of caspase-9, caspase-8 and caspase-3 *via* measurement of their active forms, respectively. As shown in Fig. 6, compound **3e** treatment significantly increased the activity of caspase-9, caspase-8 and caspase-3. When A549 cells were treated with 100 μM of compound **3e,** the activity of caspase-3 increased by 5.24 ± 0.36 ($P < .01$) fold, caspase-8 increased by the 2.98 ± 0.48 ($P < .01$), and caspase-9 increased by the 1.81 ± 0.41 ($P < .01$) compared with the control group. These results demonstrate that compound **3e** could increase the levels of activated caspase in a dose-dependent manner and induce A549 cell death by mitochondrial apoptotic pathway. Besides, compound **3e** may be considered as promising apoptotic inducer in A549 cells for future studies.

2.2.6. Expression of apoptosis-related protein treatment in A549 cells after compound *3e* treatment

Apoptosis is the result of a series of gene activation, expression and regulation changes. Therefore, we examined the expression levels of the apoptosis-related proteins Bcl-2, Bax, Cyt c, Akt, 5-Lox, p53, p21 and MDM2 to explore the mechanism by which compound **3e** treatment induces apoptosis in A549 cells. As shown in Fig. 7, compound **3e** treatment significantly downregulated Bcl-2, Akt, 5-Lox and MDM2 and upregulated the expression of Bax, Cyt c, p53 and p21 proteins in a dose- and time-dependent manner. All of these results demonstrate that compound **3e** may induce apoptosis in A549 cells *via* the p53 signaling pathway.

2.2.7. Molecular docking of compound *3e* with related proteins

Based on the *in vitro* inhibition results, compound **3e** was selected as a ligand, and molecular docking studies were further performed to explore the binding modes of compound **3e** with related proteins Akt, 5-Lox and MDM2 using AutoDock Vina. The generated docked complexes were examined on the basis of minimum energy values (kcal/mol) and bonding interaction pattern such as hydrophobic and hydrogen bonds, respectively. Hydrophobic and hydrogen bonds play an important role in molecular docking because they help to stabilize and strengthen the docked complexes.

The theoretical binding mode between compound **3e** and binding site were shown in Fig. 8A–C, Table 3. Docking of compound **3e** in Akt (Fig. 8A) showed hydrogen bonding interaction benzene ring with amino acids Arg4 (d = 3.5 Å), Lys179 (d = 3.4 Å), Asp292 (d = 2.5 Å), and Gly159 (d = 3.0 Å), and showed hydrophobic interaction with Phe438 and Met281. As shown in Fig. 8B, the bromobenzene ring of compound **3e** exhibited hydrophobic interaction with Pro569, Val604, and Phe359, and exhibited hydrogen bonding with amino acid Asn180 (d = 3.1 Å). Similarly, compound **3e** also exhibited hydrogen bonding interaction with amino acids His96 (d = 3.2 Å) and Gln18 (d = 3.0 Å) of MDM2 was depicted in Fig. 8C.

2.2.8. Compound *3e* inhibits the migration and invasion of A549 cells

The migration of tumour cells plays an important role in the late stage of cancer.[43] In early studies, we found that compound **3e** could induce the apoptosis of A549 cells. Thus, we adopted the wound-healing assay to evaluate the lateral migration ability of A549 cells after treatment with compound **3e**. As shown in Fig. 9, compound **3e** treatment significantly inhibited wound healing in a dose-dependent manner. Furthermore, we evaluated the ability of compound **3e** to inhibit longitudinal migration using transwell and Matrigel transwell assays (Fig. 10). The results also demonstrated that compound **3e** could inhibit the migration and invasion of A549 cells in a dose-dependent manner.

3. Conclusions

In conclusion, based on molecular hybridization, we designed and synthesized a promising class of novel structurally diverse chrysin-chromene-spirooxindole hybrids. The newly synthesized compounds were evaluated for their *in vitro* anticancer activity, and some of the compounds showed stronger anti-proliferative activity against A549, H1299, K562 and PC-3 than parent compound chrysin. In particular, compound **3e** had the highest cytotoxicity towards A549 cells, and had

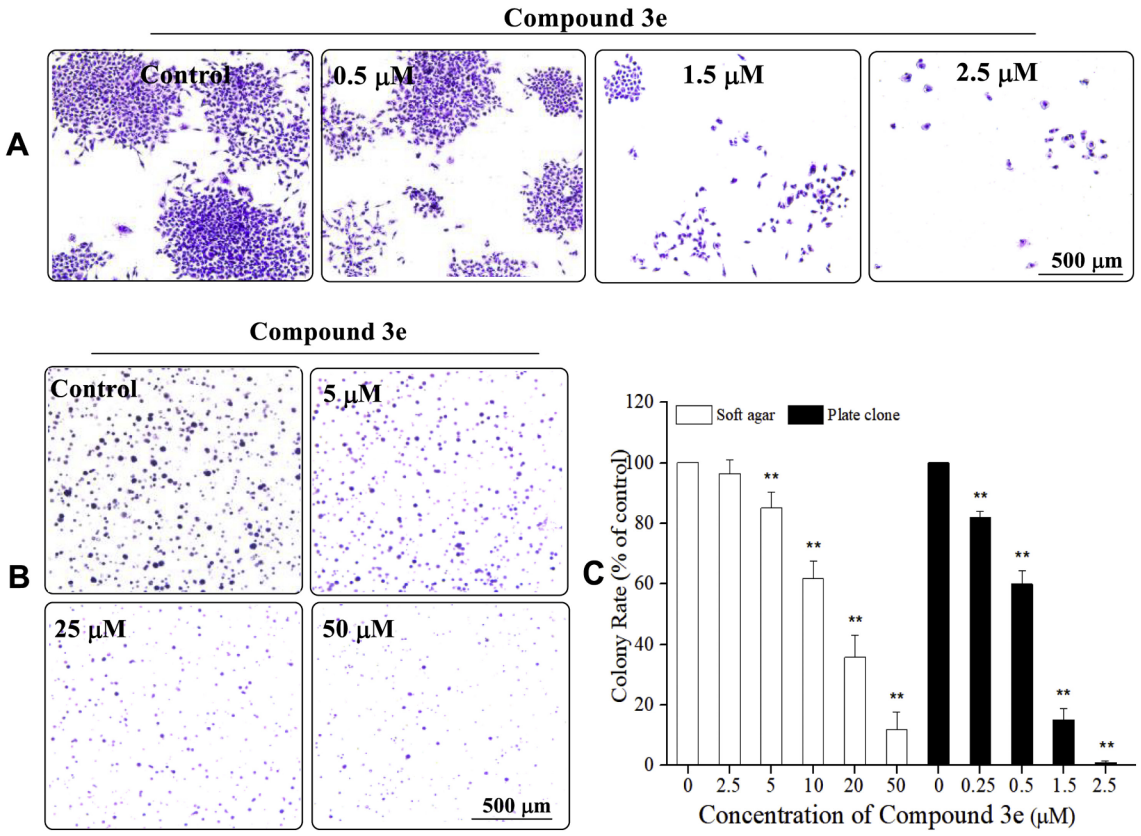

Fig. 3. (A) The plate colony formation of A549 cells were treated with compound **3e** at different concentrations for 10 days; (B) The soft agar colony formation of A549 cells were treated with compound **3e** at different concentrations for 20 days; (C) Data were represented as means ± SD obtained in at least three independent experiment. $^{*}P < .05$; $^{**}P < .01$ compared with the control group.

better selectivity in A549 cells and normal MRC-5 cells.

Preliminary mechanism studies demonstrated that compound **3e** could significantly inhibit A549 colony formation and alter cell morphology to induce cell apoptosis, which may be dependent on mitochondria-mediated caspase activation. It appears that compound **3e** treatment increased Bax and decreased Bcl-2 protein levels, thus increasing the ratio of Bax/Bcl-2, releasing cytochrome *c* and activating caspase to cause apoptosis. Simultaneously, compound **3e** treatment regulated the expression of MDM2, p21, Akt and 5-lox proteins associated with the tumour suppressor p53, thereby inducing cell death. Our results demonstrate that compound **3e** could significantly induce apoptosis and inhibit the migration and invasion of A549 cells. Apoptosis may be the result of mitochondria- mediated caspase-3/8/9 activation and multi-target co-regulation of the p53 signaling pathway. In addition, the molecular docking of active compound **3e** was also investigated. The **3e** interact with the receptor through hydrophobic hydrophobic interaction and hydrogen bonding with essential amino acid. Thus, our results provide evidence that the most active compound of this series was **3e**, which represents a good lead for drug development.

4. Experimental section

4.1. General

The ^{1}H NMR spectra were recorded on Bruker Avance DMX 400 or 500 MHz NMR spectrometers in DMSO-d_6 using TMS as an internal standard. The ^{13}C NMR spectra were recorded on Bruker Avance DMX 100 MHz NMR spectrometers in DMSO-d_6 using TMS as an internal standard. Chemical shifts were reported as δ values (ppm). High-resolution mass spectra (HRMS-ESI) were obtained on a Micro™ Q-TOF Mass Spectrometer. Melting points were uncorrected and recorded on an Electrothermal 9100 digital melting point apparatus.

Reagents were purchased from commercial sources and were used as received unless stated otherwise. Reactions were monitored by thin layer chromatography using silica gel GF_{254} plates. Column chromatography was performed on silica gel (300–400 mesh).

4.2. General procedure for synthesis of compounds 3a-z

A mixture of isatin **2** (0.8 mmol), malononitrile (1.0 mmol) and Ca$(OH)_2$ (0.8 mmol, 59.2 mg) in 5.0 mL of methanol was stirred at room temperature for 10 min followed by the addition of chrysin **1** (0.5 mmol), which was stirred under reflux for 8 h. After completion of the reaction, as indicated by TLC, the mixture was cooled to room temperature and then purified by flash chromatography to afford the corresponding product **3**.

4.2.1. 2′-Amino-5′-hydroxy-1-methyl-2,6′-dioxo-8′-phenyl-6′H-spiro [indoline-3,4′-pyrano[3,2- g] chromene]-3′-carbonitrile (3a)

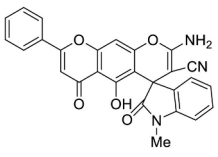

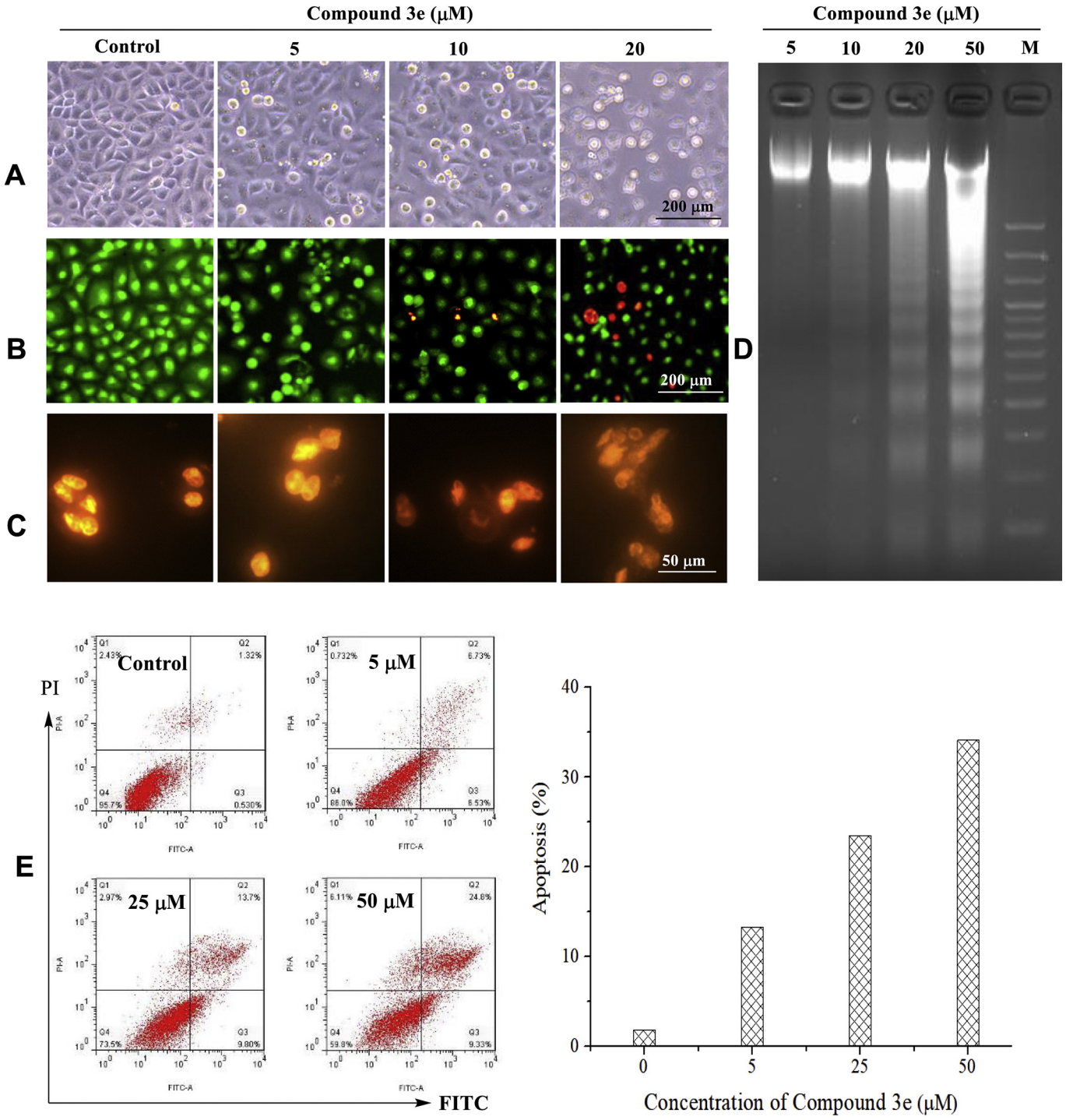

Fig. 4. Compound **3e** induced apoptosis of cells. A549 cells were treated with various concentrations of compound **3e** for 24 h. (A) Morphological observation; (B) AO-EB double staining assay; (C) PI staining assay; (D) The compound **3e**-induced apoptosis was examined by observation of the formation of DNA ladder; (E) The compound **3e**-induced apoptosis was evidenced by flow cytometry and Annexin V-FITC/PI double staining.

Yellow solid; m.p. > 300 °C; yield 72%; ^{1}H NMR (DMSO-d_6, 500 MHz) δ: 3.22 (s, 3H), 6.98–7.00 (m, 1H), 7.03–7.04 (m, 2H), 7.06–7.09 (m, 2H), 7.28–7.31 (m, 1H), 7.39 (s, 2H), 7.57–7.60 (m, 2H), 7.62–7.64 (m, 1H), 8.12 (d, J = 7.5 Hz, 2H), 13.32 (br s, 1H); ^{13}C NMR (DMSO-d_6, 125 MHz) δ: 30.7, 46.9, 55.8, 103.9, 105.23, 106.7, 108.4, 117.5, 122.8, 123.4, 126.7, 128.7, 129.2, 130.3, 132.5, 133.2, 143.6, 153.8, 155.7, 159.5, 176.1, 182.4; HRMS (ESI-TOF) m/z: Calcd. for $C_{27}H_{18}N_3O_5$ $[M + H]^+$: 464.1241; Found: 464.1242.

4.2.2. 2′-Amino-5′-hydroxy-1,5-dimethyl-2,6′-dioxo-8′-phenyl-6′H-spiro [indoline-3,4′-pyrano [3,2-g]chromene]-3′-carbonitrile (3b)

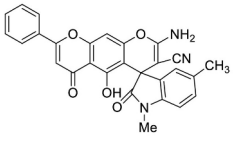

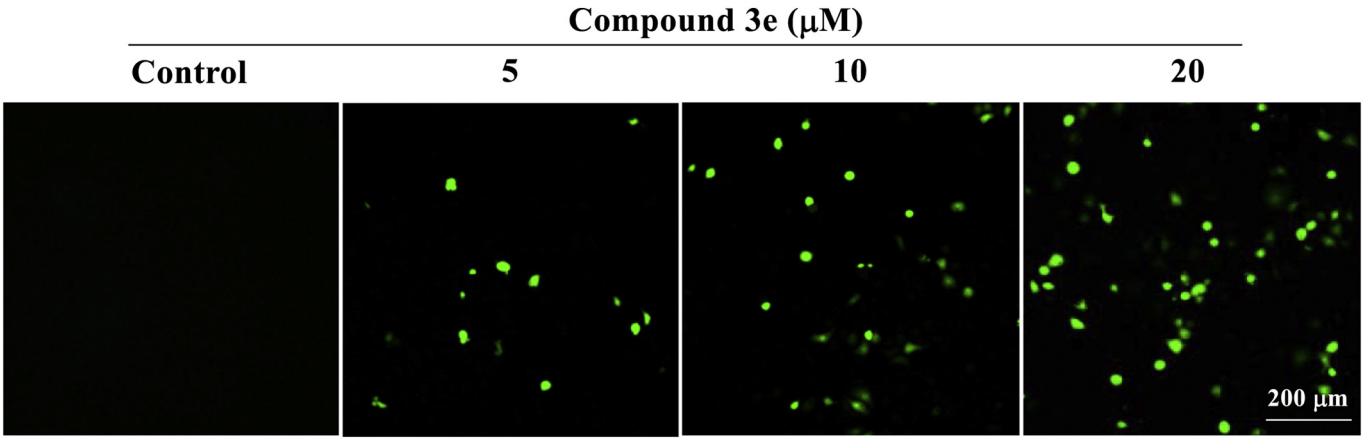

Fig. 5. Effect of compound **3e** on the production of ROS in A549 cells. Cells were treated with various concentrations of compound **3e** for 24 h and detected by examining the fluorescence of DCF in cells by the fluorescence microscope.

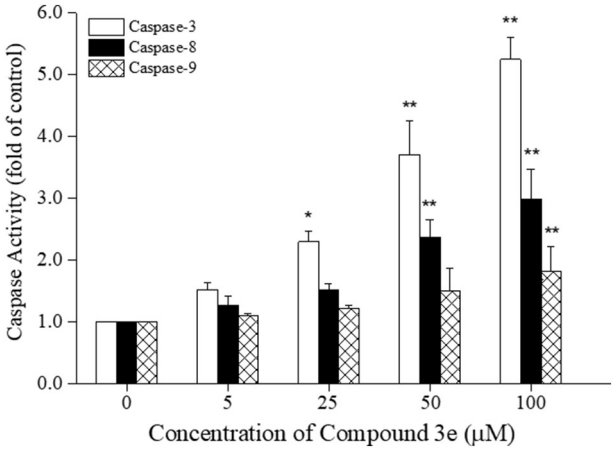

Fig. 6. A549 cells were treated with various concentrations of compound **3e** for 24 h, the effects of compound **3e** on activation of caspase-9, caspase-8 and caspase-3, respectively. Data were represented as means ± SD obtained in at least three independent experiment. $^{*}P < .05$; $^{**}P < .01$ compared with the control group.

Yellow solid; m.p. > 300 °C; yield 71%; ^{1}H NMR (DMSO-d_6, 400 MHz) δ: 2.20 (s, 3H), 3.19 (s, 3H), 6.86 (s, 1H), 6.95 (d, J = 7.9 Hz, 1H), 7.04 (s, 1H), 7.10 (d, J = 8.1 Hz, 2H), 7.37 (s, 2H), 7.56–7.65 (m, 3H), 8.12 (d, J = 7.3 Hz, 2H), 13.32 (br s, 1H); ^{13}C NMR (DMSO-d_6, 100 MHz) δ: 20.6, 26.6, 47.1, 56.0, 95.1, 104.0, 105.3, 106.7, 108.2, 117.6, 124.0, 126.8, 129.0, 129.2, 130.3, 131.8, 132.6, 133.3, 141.3, 153.8, 155.6, 158.2, 159.5, 164.4, 176.0, 182.5; HRMS (ESI-TOF) *m/z*: Calcd. for C28H20N3O5 $[M + Na]^+$: 478.1397; Found: 478.1390.

4.2.3. 2′-Amino-7-chloro-5′-hydroxy-1-methyl-2,6′-dioxo-8′-phenyl-6′H-spiro[indoline-3,4′- pyrano[3,2-g]chromene]-3′-carbonitrile (3c)

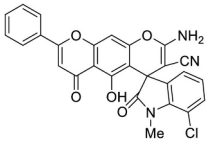

Yellow solid; m.p. > 300 °C; yield 86%; ^{1}H NMR (DMSO-d_6, 400 MHz) δ: 3.54 (s, 3H), 6.97–7.06 (m, 3H), 7.28–7.30 (m, 1H), 7.50–7.60 (m, 3H), 8.06 (d, J = 7.2 Hz, 3H), 8.05 (br s, 2H), 13.38 (br s, 1H); ^{13}C NMR (DMSO-d_6, 100 MHz) δ: 30.2, 47.4, 55.8, 95.6, 107.1, 114.3, 114.5, 117.1, 117.8, 123.3, 124.6, 127.0, 129.5, 130.6, 131.1, 132.9, 136.7, 139.6, 154.0, 156.2, 158.6, 159.0, 159.9, 164.8, 177.1, 182.7; HRMS (ESI-TOF) *m/z*: Calcd. for $C_{27}H_{17}ClN_3O_5$ $[M + H]^+$: 498.0851; Found: 498.0855.

4.2.4. 2′-Amino-5-chloro-5′-hydroxy-1-methyl-2,6′-dioxo-8′-phenyl-6′H-spiro[indoline-3,4′- pyrano[3,2-g]chromene]-3′-carbonitrile (3d)

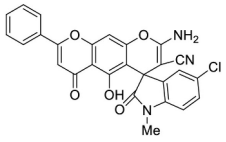

Yellow solid; m.p. > 300 °C; yield 84%; ^{1}H NMR (DMSO-d_6, 400 MHz) δ: 3.21 (s, 3H), 6.76 (br s, 2H), 7.04 (d, J = 14.8 Hz, 2H), 7.10 (d, J = 8.4 Hz, 1H), 7.21 (s, 1H), 7.34–7.36 (m, 1H), 7.47 (s, 1H), 7.53–7.62 (m, 3H), 8.09 (d, J = 7.2 Hz, 1H), 13.35 (br s, 1H); ^{13}C NMR (DMSO-d_6, 100 MHz) δ: 26.8, 47.4, 55.3, 95.4, 103.3, 105.4, 106.8, 110.0, 114.4, 116.7, 117.6, 123.9, 126.8, 128.8, 129.3, 130.4, 132.7, 135.3, 142.7, 154.0, 155.9, 158.5, 158.8, 159.8, 164.6, 176.1, 182.5; HRMS (ESI-TOF) *m/z*: Calcd. for $C_{27}H_{16}ClN_3NaO_5$ $[M + Na]^+$: 520.0671; Found: 520.0677.

4.2.5. 2′-Amino-5-bromo-5′-hydroxy-1-methyl-2,6′-dioxo-8′-phenyl-6′H-spiro[indoline-3,4′- pyrano[3,2-g]chromene]-3′-carbonitrile (3e)

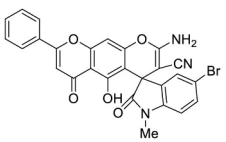

Yellow solid; m.p. > 300 °C; Yield 87%; ^{1}H NMR (DMSO-d_6, 500 MHz) δ: 3.22 (s, 3H), 7.00 (s, 1H), 7.05–7.08 (m, 2H), 7.33 (s, 1H), 7.49 (d, J = 6.9 Hz, 3H), 7.52–7.55 (m, 2H), 7.58–7.61 (m, 1H), 8.07 (d, J = 7.6 Hz, 2H), 13.34 (br s, 1H); ^{13}C NMR (DMSO-d_6, 125 MHz) δ: 31.2, 47.7, 55.6, 95.7, 103.6, 105.7, 107.2, 111.0, 115.1, 118.0, 126.9, 127.2, 129.7, 130.7, 132.0, 133.1, 136.0, 143.5, 154.3, 156.3, 158.7, 160.2, 164.9, 176.3, 182.9, 207.1; HRMS (ESI-TOF) m/z: Calcd. for $C_{27}H_{17}BrN_3O_5$ $[M + H]^+$: 542.0346; Found: 542.0344.

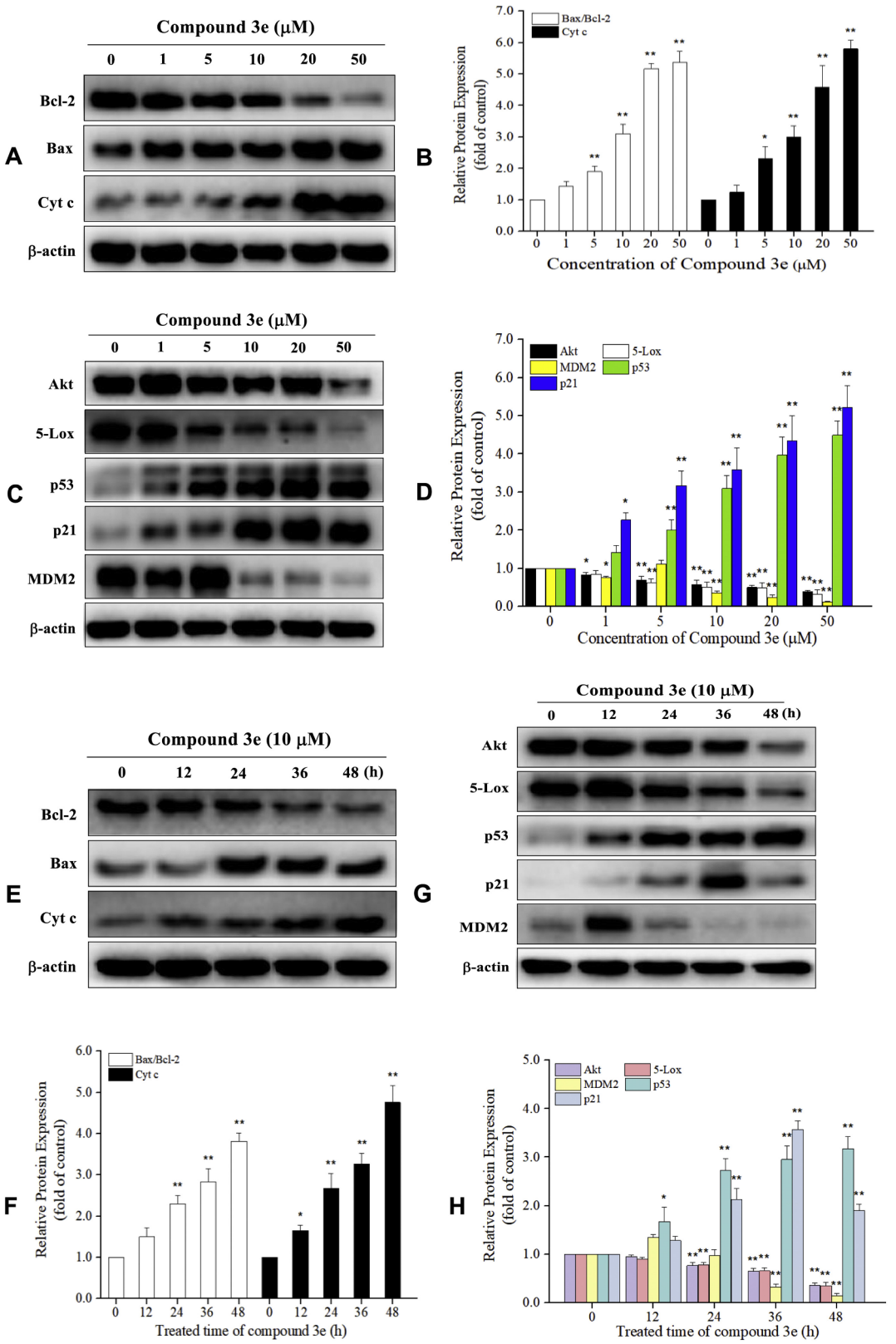

Fig. 7. Expression level of apoptosis-related protein, Bax, Bcl-2, Cyt c, p53, p21, MDM2, Akt and 5-Lox. (A-D) A549 cells were treated with compound **3e** at different concentrations for 24 h; (*E*-H) A549 cells were treated with 10 μM of compound **3e** for different time. Data were represented as means ± SD obtained in at least three independent experiments. $^{*}P < .05$; $^{**}P < .01$ verse the control group. The grayscale assay was quantified using Image Lab software.

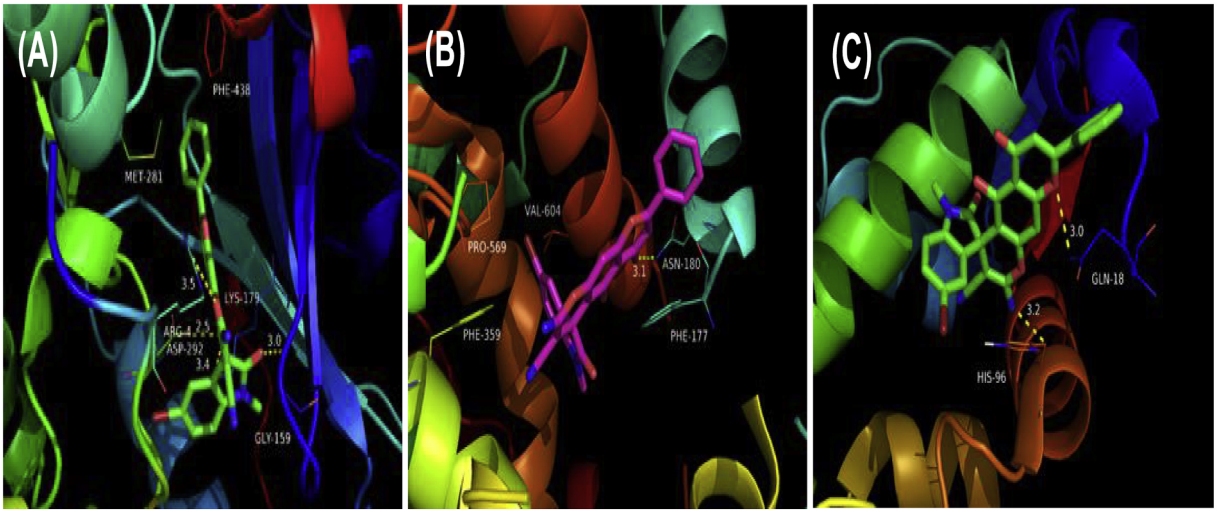

Fig. 8. (A–B) The theoretical binding models of compound **3e** with Akt, 5-Lox and MDM2. (A) Molecular docked model of compound **3e** with Akt (PDB ID: 3MV5); (B) Molecular docked model of compound **3e** with 5-Lox (PDB ID: 3V99); (C) Hydrogen bonding interactions between compound **3e** and key amino acid residues of MDM2 (PDB ID: 4ZYF).

Table 3
Binding affinities of compound **3e** to related proteins by molecular docking.

Docking model	Docking score (kcal/mol)
Akt	−5.6
5-Lox	−6.4
MDM2	−5.4

4.2.6. 2′-Amino-1-benzyl-5′-hydroxy-5-methyl-2,6′-dioxo-8′-phenyl-6′H-spiro[indoline-3,4′- pyrano[3,2-g]chromene]-3′-carbonitrile (3f)

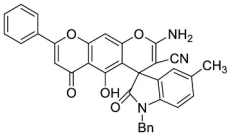

Yellow solid; m.p. > 300 °C; yield 78%; ^{1}H NMR (DMSO-d_6, 500 MHz) δ: 2.16 (s, 3H), 4.91 (d, J = 15.8 Hz, 1H), 5.03 (d, J = 15.9 Hz, 1H), 6.74 (d, J = 8.0 Hz, 1H), 6.90 (s, 1H), 6.98 (d, J = 7.9 Hz, 3H), 7.25–7.28 (m, 1H), 7.30–7.33 (m, 2H), 7.44–7.55 (m, 7H), 8.05 (br s, 2H), 13.35 (br s, 1H); ^{13}C NMR (DMSO-d_6, 125 MHz) δ: 20.6, 43.7, 47.3, 56.2, 95.2, 10.3.9, 105.2, 106.7, 108.9, 117.9, 124.3, 126.7, 127.4, 127.6, 128.4, 128.9, 129.2, 130.2, 132.1, 132.6, 133.4, 136.3, 140.5, 153.9, 155.7, 158.5, 159.7, 164.5, 176.4, 182.5; HRMS (ESI-TOF) m/z: Calcd. for $C_{34}H_{24}N_3O_5$ [M + H]$^+$: 554.1710; Found: 554.1713.

4.2.7. 2′-Amino-1-benzyl-5′-hydroxy-7-methyl-2,6′-dioxo-8′-phenyl-6′H-spiro[indoline-3,4′- pyrano[3,2-g]chromene]-3′-carbonitrile (3g)

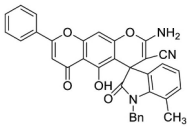

Yellow solid; m.p. > 300 °C; yield 75%; ^{1}H NMR (DMSO-d_6, 500 MHz) δ: 2.23 (s, 3H), 5.14 (d, J = 17.4 Hz, 1H), 5.26 (d, J = 17.2 Hz, 1H), 6.88–6.93 (m, 2H), 6.98 (d, J = 6.9 Hz, 1H), 7.05 (d, J = 14.2 Hz, 2H), 7.25–7.28 (m, 1H), 7.32–7.35 (m, 2H), 7.42 (d, J = 7.5 Hz, 2H), 7.53–7.56 (m, 2H), 7.59–7.61 (m, 1H), 8.09 (d, J = 7.6 Hz, 2H), 9.73 (br s, 2H), 13.54 (br s, 1H); ^{13}C NMR (DMSO-d_6, 125 MHz) δ: 18.1, 45.3, 46.8, 56.5, 95.2, 104.5, 105.3, 106.8, 114.0, 116.3, 118.1, 119.2, 122.0, 123.1, 126.0, 126.8, 127.1, 128.6, 129.2, 130.3, 132.5, 134.3, 138.4, 141.0, 153.9, 155.8, 158.0, 158.3, 158.5, 158.6, 159.6, 164.6, 177.6, 182.6; HRMS (ESI-TOF) m/z: Calcd. for $C_{34}H_{24}N_3O_5$ [M + H]$^+$: 554.1710; Found: 554.1712.

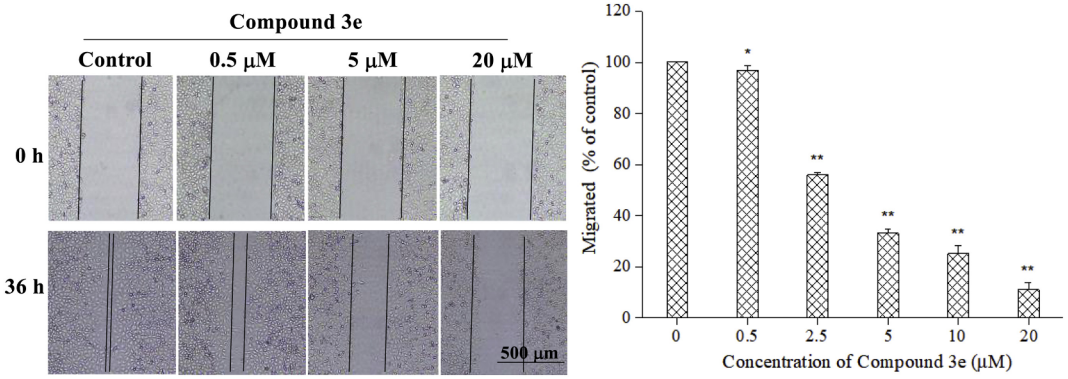

Fig. 9. With different concentrations of compound **3e** inhibits migration abilities of A549 cells by using wound healing assay. Data were represented as means ± SD obtained in at least three independent experiments. $^{*}P < .05$; $^{**}P < .01$ verse the control group.

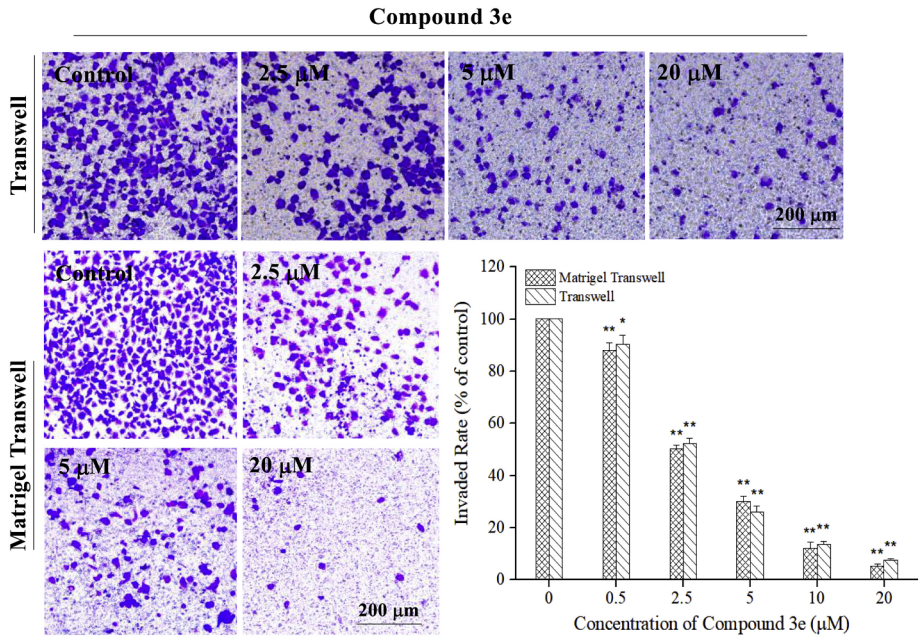

Fig. 10. With different concentrations of compound **3e** inhibits migration and invasion abilities of A549 cells by using transwell and matrigel transwell assay. Data were represented as means ± SD obtained in at least three independent experiments. $^{*}P < .05$; $^{**}P < .01$ verse the control group.

4.2.8. 2′-Amino-1-benzyl-5′-hydroxy-5-methoxy-2,6′-dioxo-8′-phenyl-6′H-spiro[indoline-3,4′- pyrano[3,2-g]chromene]-3′-carbonitrile (3h)

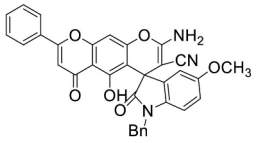

Yellow solid; m.p. > 300 °C; yield 71%; ^{1}H NMR (DMSO-d_6, 400 MHz) δ:; ^{13}C NMR (DMSO-d_6, 100 MHz) δ: 44.1, 48.4, 54.6, 57.9, 106.9, 107.5, 107.7, 108.5, 111.9, 119.4, 126.5, 127.3, 128.7, 129.6, 131.3, 132.1, 136.1, 136.5, 137.4, 154.4, 154.9, 159.1, 160.3, 161.2, 168.9, 178.1, 180.1; HRMS (ESI-TOF) *m/z*: Calcd. for $C_{34}H_{24}N_3O_6$ $[M + H]^+$: 570.1660; Found: 570.1660.

4.2.9. 2′-Amino-1-benzyl-5-fluoro-5′-hydroxy-2,6′-dioxo-8′-phenyl-6′H-spiro[indoline-3,4′- pyrano[3,2-g]chromene]-3′-carbonitrile (3i)

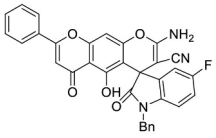

Yellow solid; m.p. > 300 °C; yield 85%; ^{1}H NMR (DMSO-d_6, 500 MHz) δ: 4.93 (d, J = 15.9 Hz, 1H), 5.04 (d, J = 15.9 Hz, 1H), 6.19 (br s, 2H), 6.85–6.88 (m, 1H), 7.03–7.06 (m, 3H), 7.10–7.12 (m, 1H), 7.27–7.29 (m, 1H), 7.31–7.34 (m, 1H), 7.46–7.62 (m, 6H), 8.10 (d, J = 7.4 Hz, 2H), 13.41 (br s, 1H); ^{13}C NMR (DMSO-d_6, 125 MHz) δ: 43.7, 47.6, 55.3, 95.2, 103.2, 105.3, 106.7, 109.9, 111.7, 111.9, 114.8, 115.0, 117.7, 126.7, 127.5, 128.4, 129.2, 130.2, 132.6, 135.0, 135.9, 139.0, 153.9, 155.8, 158.0, 158.3, 158.4, 158.7, 159.8, 159.9, 164.5, 176.4, 182.5; HRMS (ESI-TOF) *m/z*: Calcd. for $C_{33}H_{21}FN_3O_5$ $[M + H]^+$: 558.1460; Found: 558.1458.

4.2.10. 2′-Amino-1-benzyl-5-chloro-5′-hydroxy-2,6′-dioxo-8′-phenyl-6′H-spiro[indoline-3,4′- pyrano[3,2-g]chromene]-3′-carbonitrile (3j)

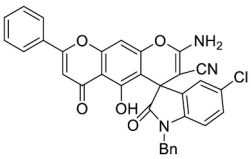

Yellow solid; m.p. > 300 °C; yield 86%; ^{1}H NMR (DMSO-d_6, 500 MHz) δ: 4.93 (d, J = 16.0 Hz, 1H), 5.04 (d, J = 15.9 Hz, 1H), 6.88–6.90 (m, 1H), 7.06 (d, J = 10.5 Hz, 2H), 7.26–7.34 (m, 5H), 7.45 (d, J = 7.1 Hz, 2H), 7.53–7.62 (m, 5H), 8.10–8.11 (m, 2H), 13.41 (br s, 1H); ^{13}C NMR (DMSO-d_6, 125 MHz) δ: 43.7, 47.4, 55.1, 95.3, 103.1, 105.3, 106.7, 110.5, 117.7, 124.1, 126.8, 127.1, 127.5, 128.5, 128.6, 129.2, 130.3, 132.6, 135.3, 135.8, 141.7, 153.9, 155.9, 158.1, 158.3, 159.8, 164.5, 176.2, 182.5; HRMS (ESI-TOF) *m/z*: Calcd. for $C_{33}H_{21}ClN_3O_5$ $[M + H]^+$: 574.1164; Found: 574.1169.

4.2.11. 2′-Amino-1-benzyl-5-bromo-5′-hydroxy-2,6′-dioxo-8′-phenyl-6′H-spiro[indoline-3,4′- pyrano[3,2-g]chromene]-3′-carbonitrile (3k)

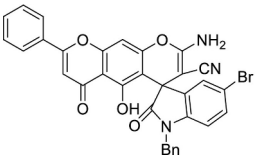

Yellow solid; m.p. > 300 °C; yield 84%; ^{1}H NMR (DMSO-d_6, 400 MHz) δ: 4.90 (d, J = 15.9 Hz, 1H), 5.01 (d, J = 15.9 Hz, 1H), 6.82 (d, J = 8.4 Hz, 1H), 7.02 (s, 1H), 7.06 (s, 1H), 7.25–7.43 (m, 7H), 7.49 (s, 2H), 7.52–7.61 (m, 3H), 8.09 (d, J = 7.3 Hz, 2H), 13.39 (br s, 1H); ^{13}C NMR (DMSO-d_6, 100 MHz) δ: 44.1, 47.8, 55.6, 95.8, 103.5, 105.8,

107.1, 111.5, 115.3, 118.2, 127.2, 128.0, 128.9, 129.7, 130.7, 131.9, 133.1, 136.0, 136.2, 142.6, 154.4, 156.3, 158.8, 160.3, 164.9, 176.6, 183.0; HRMS (ESI-TOF) *m/z*: Calcd. for $C_{33}H_{21}BrN_3O_5$ $[M + H]^+$: 618.0659; Found: 618.0653.

4.2.12. 2′-Amino-1-benzyl-7-chloro-5′-hydroxy-2,6′-dioxo-8′-phenyl-6′H-spiro[indoline-3,4′- pyrano[3,2-g]chromene]-3′-carbonitrile (3l)

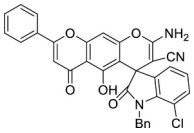

Yellow solid; m.p. > 300 °C; yield 85%; ^{1}H NMR (DMSO-d_6, 500 MHz) δ: 5.27 (d, J = 16.8 Hz, 1H), 5.33 (d, J = 16.7 Hz, 1H), 6.99–7.02 (m, 1H), 7.03 (d, J = 1.6 Hz, 2H), 7.11 (d, J = 7.3 Hz, 1H), 7.22–7.24 (m, 2H), 7.28–7.31 (m, 2H), 7.39 (d, J = 7.4 Hz, 2H), 7.52–7.55 (m, 2H), 7.57–7.60 (m, 1H), 8.07 (d, J = 7.3 Hz, 2H), 13.26 (br s, 3H); ^{13}C NMR (DMSO-d_6, 125 MHz) δ: 45.5, 47.4, 55.8, 95.7, 103.5, 107.1, 111.9, 114.2, 116.5, 118.0, 118.8, 123.4, 124.7, 126.6, 127.0, 128.6, 129.4, 130.6, 131.2, 132.8, 136.8, 138.2, 139.1, 154.0, 156.3, 158.2, 158.5, 158.8, 159.1, 160.0, 164.9, 169.4, 177.6, 182.7; HRMS (ESI-TOF) *m/z*: Calcd. for $C_{33}H_{21}ClN_3O_5$ $[M + H]^+$: 574.1164; Found: 574.1159.

4.2.13. 2′-Amino-5′-hydroxy-2,6′-dioxo-1,8′-diphenyl-6′H-spiro[indoline-3,4′-pyrano[3,2-g] chromene]-3′-carbonitrile (3 m)

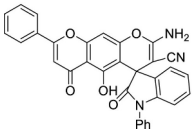

Yellow solid; m.p. > 300 °C; yield 81%; ^{1}H NMR (DMSO-d_6, 400 MHz) δ: 5.95 (br s, 2H), 6.72 (d, J = 7.9 Hz, 1H), 7.03–7.09 (m, 2H), 7.14 (d, J = 7.2 Hz, 1H), 7.21–7.25 (m, 1H), 7.44–7.64 (m, 9H), 8.11 (d, J = 7.3 Hz, 2H), 13.46 (br s, 1H); ^{13}C NMR (DMSO-d_6, 100 MHz) δ: 47.3, 56.1, 95.3, 103.8, 105.3, 106.9, 108.8, 114.3, 117.2, 117.6, 123.5, 124.1, 126.8, 128.4, 128.8, 129.2, 129.9, 130.1, 132.6, 133.0, 134.6, 143.3, 153.8, 155.8, 158.2, 158.3, 158.6, 159.5, 164.5, 175.8, 182.5; HRMS (ESI-TOF) *m/z*: Calcd. for $C_{32}H_{20}N_3O_5$ $[M + H]^+$: 526.1397; Found: 526.1402.

4.2.14. 2′-Amino-1-ethyl-5′-hydroxy-7-methyl-2,6′-dioxo-8′-phenyl-6′H-spiro[indoline-3,4′- pyrano[3,2-g]chromene]-3′-carbonitrile (3n)

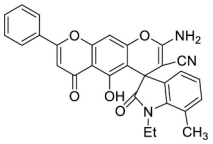

Yellow solid; m.p. > 300 °C; yield 73%; ^{1}H NMR (DMSO-d_6, 400 MHz) δ: 1.20–1.29 (m, 3H), 2.57 (s, 3H), 3.97–4.02 (m, 2H), 6.85–6.91 (m, 2H), 7.01–7.13 (m, 3H), 7.34–7.41 (m, 2H), 7.56–7.60 (m, 2H), 7.62–7.66 (m, 1H), 8.08–8.17 (m, 2H); ^{13}C NMR (DMSO-d_6, 100 MHz) δ: 14.3, 18.4, 36.5, 46.4, 56.5, 95.0, 104.2, 105.2, 106.6, 117.5, 118.7, 121.8, 122.6, 126.7, 129.1, 130.2, 132.5, 134.5, 140.4, 153.8, 155.6, 158.4, 159.4, 164.3, 176.6, 182.4; HRMS (ESI-TOF) *m/z*: Calcd. for $C_{29}H_{22}N_3O_5$ $[M + H]^+$: 492.1554; Found: 492.1551.

4.2.15. 2′-Amino-1-ethyl-5′-hydroxy-5-methyl-2,6′-dioxo-8′-phenyl-6′H-spiro[indoline-3,4′- pyrano[3,2-g]chromene]-3′-carbonitrile (3o)

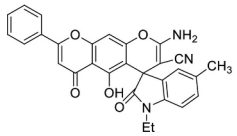

Yellow solid; m.p. > 300 °C;, yield 75%; ^{1}H NMR (DMSO-d_6, 500 MHz) δ: 1.18–1.21 (m, 3H), 2.19 (s, 3H), 3.76–3.78 (m, 2H), 6.87 (s, 1H), 6.98–7.02 (m, 2H), 7.08 (d, J = 7.5 Hz, 1H), 7.37 (br s, 2H), 7.50–7.59 (m, 3H), 8.05–8.06 (m, 2H), 13.30 (br s, 1H); ^{13}C NMR (DMSO-d_6, 125 MHz) δ: 12.2, 20.6, 34.5, 47.0, 56.3, 95.0, 104.0, 105.3, 106.7, 108.2, 117.5, 124.2, 126.0, 126.7, 129.2, 130.3, 131.6, 132.5, 133.6, 140.1, 153.9155.6, 158.5, 159.5, 164.3175.5, 182.4; HRMS (ESI-TOF) *m/z*: Calcd. for $C_{29}H_{21}N_3NaO_5$ $[M + Na]^+$: 514.1373; Found: 514.1379.

4.2.16. tert-Butyl 2-(2′-amino-3′-cyano-5′-hydroxy-2,6′-dioxo-8′-phenyl-6′H-spiro[indoline- 3,4′-pyrano [3,2-g]chromene]-1-yl)acetate (3p)

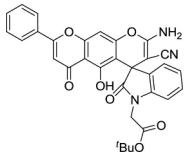

Yellow solid; m.p. > 300 °C; yield 77%; ^{1}H NMR (DMSO-d_6, 500 MHz) δ: 1.40 (s, 9H), 4.41 (d, J = 17.0 Hz, 1H), 4.48 (d, J = 17.0 Hz, 1H), 6.97–7.01 (m, 4H), 7.06 (d, J = 6.7 Hz, 1H), 7.24–7.28 (m, 1H), 7.49–7.52 (m, 2H), 7.54–7.57 (m, 1H), 8.03 (d, J = 7.3 Hz, 2H), 11.24 (br s, 2H), 13.23 (br s, 1H); ^{13}C NMR (DMSO-d_6, 125 MHz) δ: 27.9, 43.2, 47.4, 56.2, 82.0, 95.5, 107.0, 109.3, 112.0, 114.3, 116.6, 117.6, 118.9, 123.3, 123.9, 127.0, 128.8, 129.5, 130.7, 132.8, 133.3, 143.1, 156.2, 158.4, 158.7, 159.0, 159.3, 160.1, 166.9, 176.4, 182.7; HRMS (ESI-TOF) *m/z*: Calcd. for $C_{32}H_{25}N_3NaO_7$ $[M + Na]^+$: 586.1585; Found: 586.1579.

4.2.17. 2′-Amino-5′-hydroxy-2,6′-dioxo-8′-phenyl-6′H-spiro[indoline-3,4′-pyrano[3,2-g] chromene]-3′-carbonitrile (3q)

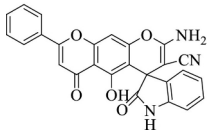

Yellow solid; m.p. > 300 °C; yield 74%; ^{1}H NMR (DMSO-d_6, 500 MHz) δ: 6.88 (d, J = 10.0 Hz, 1H), 6.93 (d, J = 9.0 Hz, 1H), 6.99 (d, J = 8.5 Hz, 1H), 7.03 (s, 1H), 7.08 (s, 1H), 7.19–7.22 (m, 1H), 7.31 (s, 2H), 7.55–7.64 (m, 3H), 8.12 (d, J = 9.0 Hz, 2H), 10.64 (br s, 1H), 13.4 (br s, 1H); ^{13}C NMR (DMSO-d_6, 125 MHz) δ: 47.9, 56.9, 95.4, 104.5, 105.7, 107.1, 109.8, 122.5, 124.1, 127.2, 129.0, 129.6, 130.8, 134.5, 142.6, 154.4, 156.1, 158.9, 159.9, 164.9, 178.0, 182.9; HRMS (ESI-TOF) *m/z*: Calcd. for $C_{26}H_{15}N_3NaO_5$ $[M + Na]^+$: 472.0904; Found: 472.0891.

4.2.18. 2′-Amino-5′-hydroxy-5-methyl-2,6′-dioxo-8′-phenyl-6′H-spiro [indoline-3,4′-pyrano [3,2-g]chromene]-3′-carbonitrile (3r)

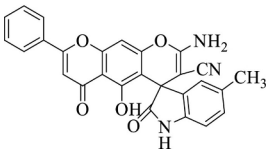

Yellow solid; m.p. > 300 °C; yield 70%; ^{1}H NMR (DMSO-d_6, 500 MHz) δ: 1.66 (s, 3H), 6.28 (s, 1H), 6.35 (s, 1H), 6.41 (s, 1H), 6.93–6.96 (m, 3H), 7.54–7.56 (m, 4H), 8.01–8.03 (m, 2H); ^{13}C NMR (DMSO-d_6, 125 MHz) δ: 20.8, 48.9, 57.5, 106.6, 106.8, 109.7, 112.4, 118.9, 123.1, 126.2, 126.8, 129.5, 129.8, 131.7, 135.8, 140.2, 154.2, 159.1, 160.4, 160.5, 169.3, 179.1, 182.1; HRMS (ESI-TOF) *m/z*: Calcd. for $C_{27}H_{17}N_3NaO_5$ [M + Na]$^+$: 486.1060; Found: 486.1049.

4.2.19. 2′-Amino-7-chloro-5′-hydroxy-2,6′-dioxo-8′-phenyl-6′H-spiro [indoline-3,4′-pyrano [3,2-g]chromene]-3′-carbonitrile (3s)

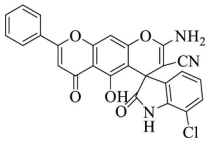

Yellow solid; m.p. > 300 °C; yield 77%; ^{1}H NMR (DMSO-d_6, 500 MHz) δ: 6.21 (s, 1H), 6.68 (s, 1H), 6.71–6.74 (m, 2H), 6.97–7.00 (m, 3H), 7.58–7.59 (m, 3H), 8.01–8.03 (m, 2H), 10.20 (br s, 1H); ^{13}C NMR (DMSO-d_6, 125 MHz) δ: 49.3, 57.8, 106.3, 107.3, 111.5, 113.7, 118.7, 121.8, 122.7, 126.4, 129.6, 131.5, 131.9, 138.0, 154.5, 159.1, 160.3, 169.1, 179.6; HRMS (ESI-TOF) *m/z*: Calcd. for $C_{26}H_{14}ClN_3NaO_5$ [M + Na]$^+$: 506.0514; Found: 506.0504.

4.2.20. 2′-Amino-6-chloro-5′-hydroxy-2,6′-dioxo-8′-phenyl-6′H-spiro [indoline-3,4′-pyrano [3,2-g]chromene]-3′-carbonitrile (3 t)

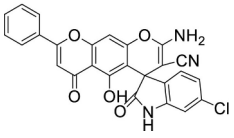

Yellow solid; m.p. > 300 °C; yield 76%; ^{1}H NMR (DMSO-d_6, 400 MHz) δ: 6.91 (s, 1H), 6.96–7.00 (m, 2H), 7.05–7.07 (m, 2H), 7.43 (br s, 2H), 7.53–7.62 (m, 3H), 8.07–8.10 (m, 2H), 10.86 (br s, 1H), 13.45 (br s, 1H); ^{13}C NMR (DMSO-d_6, 100 MHz) δ: 47.6, 56.1, 95.5, 103.8, 105.7, 107.1, 109.9, 118.0, 122.3, 125.7, 127.1, 129.6, 130.6, 133.2, 133.3, 144.1, 154.3, 156.1, 158.8, 159.9, 164.8, 178.1, 182.8; HRMS (ESI-TOF) *m/z*: Calcd. for $C_{26}H_{14}ClN_3NaO_5$ [M + Na]$^+$: 506.0514; Found: 506.0502.

4.2.21. 2′-Amino-6-bromo-5′-hydroxy-2,6′-dioxo-8′-phenyl-6′H-spiro [indoline-3,4′-pyrano [3,2-g]chromene]-3′-carbonitrile (3u)

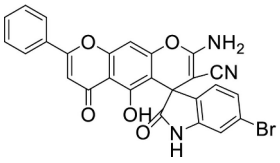

Yellow solid; m.p. > 300 °C; yield 75%; ^{1}H NMR (DMSO-d_6, 400 MHz) δ: 6.99–7.05 (m, 3H), 7.10–7.13 (m, 2H), 7.43 (br s, 2H), 7.59–7.65 (m, 3H), 8.13 (d, J = 7.2 Hz, 2H), 10.83 (br s, 1H), 13.47 (br s, 1H); ^{13}C NMR (DMSO-d_6, 100 MHz) δ: 47.7, 56.0, 95.6, 103.8, 105.7, 107.1, 112.6, 117.9, 121.5, 125.2, 126.1, 127.2, 129.6, 130.7, 133.0, 133.8, 144.2, 154.3, 156.2, 158.8, 159.9, 164.9, 178.0, 182.9; HRMS (ESI-TOF) *m/z*: Calcd. for $C_{26}H_{14}BrN_3NaO_5$ [M + Na]$^+$: 550.0009; Found: 550.0009.

4.2.22. 2′-Amino-8′-(2,4-dimethoxyphenyl)-5′-hydroxy-1,5-dimethyl-2,6′-dioxo-6′H-spiro [indoline-3,4′-pyrano[3,2-g]chromene]-3′-carbonitrile (3v)

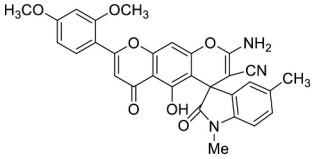

Yellow solid; m.p. > 300 °C; yield 70%; ^{1}H NMR (DMSO-d_6, 500 MHz) δ: 2.20 (s, 3H), 3.20 (s, 3H), 3.83 (d, J = 1.7 Hz, 6H), 6.62–6.67 (m, 2H), 6.84–6.88 (m, 3H), 6.95 (d, J = 8.0 Hz, 1H), 7.09 (d, J = 7.4 Hz, 1H), 7.34 (br s, 2H), 7.89 (d, J = 8.8 Hz, 1H), 13.46 (br s, 1H); ^{13}C NMR (DMSO-d_6, 125 MHz) δ: 20.6, 26.6, 47.1, 55.7, 56.0, 94.7, 98.7, 103.6, 106.2, 106.4, 107.6, 108.1, 110.9, 117.7, 124.0, 128.9, 130.5, 131.8, 133.4, 141.3, 153.6, 155.4, 158.1, 159.6, 160.0, 162.0, 163.9, 176.1, 182.2; HRMS (ESI-TOF) *m/z*: Calcd. for $C_{30}H_{24}N_3O_7$ [M + Na]$^+$: 538.1609; Found: 538.1608.

4.2.23. 2′-Amino-5-chloro-8′-(2,4-dimethoxyphenyl)-1-ethyl-5′-hydroxy-2,6′-dioxo-6′H-spiro [indoline-3,4′-pyrano[3,2-g]chromene]-3′-carbonitrile (3w)

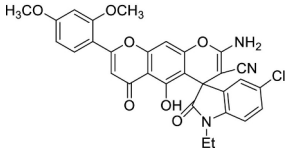

Yellow solid; m.p. > 300 °C; yield 85%; ^{1}H NMR (DMSO-d_6, 500 MHz) δ: 1.17–1.19 (m 3H), 3.74–3.82 (m, 2H), 3.84 (s, 3H), 3.86 (s, 3H), 6.66–6.69 (m, 2H), 6.89 (d, J = 8.2 Hz, 2H), 7.13 (d, J = 8.4 Hz, 1H), 7.20 (d, J = 2.0 Hz, 1H), 7.32–7.34 (m, 1H), 7.41 (br s, 2H), 7.94 (d, J = 8.8 Hz, 1H), 13.50 (br s, 1H); ^{13}C NMR (DMSO-d_6, 125 MHz) δ: 12.2, 34.9, 47.3, 55.4, 55.8, 56.1, 95.1, 99.0, 106.4, 111.1, 111.2, 111.8, 114.1, 116.4, 117.6, 118.7, 124.1, 126.9, 128.7, 130.7, 135.7, 141.6, 155.8, 158.1, 158.4, 158.8, 159.8, 160.2, 164.1, 175.7, 182.4; HRMS (ESI-TOF) *m/z*: Calcd. for $C_{30}H_{23}ClN_3O_7$ [M + Na]$^+$: 572.1219; Found: 572.1225.

4.2.24. 2′-Amino-5-bromo-8′-(2,4-dimethoxyphenyl)-1-ethyl-5′-hydroxy-2,6′-dioxo-6′H-spiro [indoline-3,4′-pyrano[3,2-g]chromene]-3′-carbonitrile (3x)

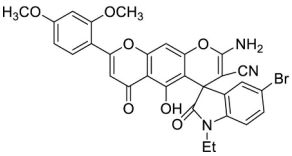

Yellow solid; m.p. > 300 °C; yield 86%; ^{1}H NMR (DMSO-d_6, 400 MHz) δ: 1.13–1.17 (m, 3H), 3.71–3.82 (m, 8H), 6.54 (s, 1H), 6.58–6.61 (m, 1H), 6.74 (s, 1H), 6.80 (s, 1H), 7.05 (d, J = 8.4 Hz, 1H), 7.30 (s, 1H), 7.42–7.44 (m, 1H), 7.83 (d, J = 8.9 Hz, 1H), 10.43 (br s, 2H), 13.47 (br s, 1H); ^{13}C NMR (DMSO-d_6, 100 MHz) δ: 12.4, 35.2, 47.5, 55.7, 56.0, 56.2, 99.1, 103.1, 106.6, 111.3, 114.1, 114.8, 116.9, 119.8, 127.1, 130.8, 131.9, 136.3, 142.3, 154.0, 156.0, 158.3, 158.7, 159.1, 159.5, 160.1, 160.4, 164.4, 175.9, 182.6; HRMS (ESI-TOF) m/z: Calcd. for $C_{30}H_{23}BrN_3O_7$ [M + H]$^+$: 616.0714; Found: 616.0722.

4.2.25. 2′-Amino-1-benzyl-8′-(2,4-dimethoxyphenyl)-5′-hydroxy-2,6′-dioxo-6′H-spiro [indoline-3,4′-pyrano[3,2-g]chromene]-3′-carbonitrile (3y)

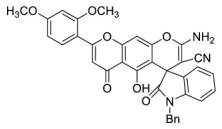

Yellow solid; m.p. > 300 °C; yield 73%; ^{1}H NMR (DMSO-d_6, 500 MHz) δ: 3.82 (d, J = 4.5 Hz, 6H), 4.91 (d, J = 15.9 Hz, 1H), 5.05 (d, J = 15.9 Hz, 1H), 6.61 (d, J = 2.1 Hz, 1H), 6.64–6.67 (m, 1H), 6.84–6.87 (m, 3H), 6.95–6.98 (m, 1H), 7.08 (d, J = 7.1 Hz, 1H), 7.16–7.19 (m, 1H), 7.24–7.28 (m, 1H), 7.30–7.33 (m, 2H), 7.47 (d, J = 7.3 Hz, 2H), 7.90 (d, J = 8.9 Hz, 1H), 8.88 (br s, 2H), 13.53 (br s, 1H); ^{13}C NMR (DMSO-d_6, 125 MHz) δ: 43.8, 47.4, 55.8, 56.1, 95.0, 98.9, 103.6, 106.4, 106.6, 109.2, 111.1, 111.9, 114.2, 116.5, 118.1, 118.7, 123.1, 123.9, 127.7, 128.6, 130.7, 133.6, 136.4, 143.0, 153.8, 155.7, 158.2, 158.5, 158.8, 159.1, 159.9, 160.2, 162.2, 164.2, 176.7, 182.4; HRMS (ESI-TOF) m/z: Calcd. for $C_{35}H_{26}N_3O_7$ $[M + H]^+$: 600.1765; Found: 600.1761.

4.2.26. 2′-Amino-1-benzyl-8′-(2-fluorophenyl)-5′-hydroxy-5-methyl-2,6′-dioxo-6′H-spiro [indoline-3,4′-pyrano[3,2-g]chromene]-3′-carbonitrile (3z)

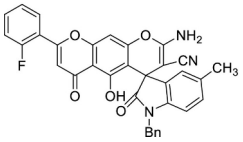

Yellow solid; m.p. > 300 °C; yield 71%; ^{1}H NMR (DMSO-d_6, 500 MHz) δ: 2.17 (s, 3H), 4.89 (d, J = 15.8 Hz, 1H), 5.01 (d, J = 15.8 Hz, 1H), 6.75 (d, J = 8.0 Hz, 1H), 6.79 (s, 1H), 6.89 (s, 1H), 6.99–7.01 (m, 2H), 7.26–7.33 (m, 3H), 7.43–7.48 (m, 6H), 7.68–7.69 (m, 1H), 8.04–8.07 (m, 1H), 13.20 (br s, 1H); ^{13}C NMR (DMSO-d_6, 125 MHz) δ: 20.6, 43.6, 47.2, 56.1, 95.1, 104.0, 106.5, 108.9, 109.8, 117.0 (d, J_{CF} = 21.3 Hz), 117.8, 118.7 (d, J_{CF} = 8.8 Hz), 124.2, 125.3, 127.5, 128.3, 128.9, 129.7, 132.0, 133.3, 134.4, 136.2, 140.4, 154.0, 155.7, 158.3, 159.6, 159.9 (d, J_{CF} = 253.8 Hz), 160.3, 176.2182.2; HRMS (ESI-TOF) m/z: Calcd. for $C_{34}H_{23}FN_3O_5$ $[M + H]^+$: 572.1616; Found: 572.1618.

4.3. Cell culture

All cell lines were purchased from the Chinese Academy of Sciences, Kunming Cell Bank. These cells were cultured in RPMI-1640 medium (Gibco, USA) supplemented with 10% foetal bovine serum (HyClone, USA) 100 U/mL penicillin and 100 mg/mL streptomycin in a humidified atmosphere with 5% CO_2 at 37 °C. The concentration of DMSO was < 0.1%, and did not have any substantial effect on cellular function. Therefore, the DMSO concentration of the mixture was controlled within this range.

4.4. MTT assay

A total of 5 × 10^3 log-phase cells were inoculated into each well of a 96-well plate in RPMI-1640 medium (Nest Biotechnology, China) and incubated for 24 h. The different concentrations of compounds were added to each well and incubated for another 48 h. Next, 10 μL of MTT reagent (5 mg/mL) was added to each well to react with the mitochondria of living cells for approximately 4 h. Finally, the medium was discarded, and the blue crystals were completely dissolved in 150 μL DMSO. Absorbance at the wavelength of 490 nm was read using a microplate reader. The concentration of compounds when 50% of cells were inhibited (IC_{50}) was calculated with IBM SPSS Statistics (version 19). The IC_{50} of each compound was obtained in at least three independent experiments.

4.5. Colony formation assay

Plate colony and soft agar colony formation assays were used to assess the colony forming ability of cancer cells. Both experiments were slightly modified from previously reported methods.[41,44]

For the plate colony formation assay, log-phase A549 cells were seeded in each 6-well plate (Nest Biotechnology, China) at 1 × 10^3 cells/well. After incubation for 24 h, the medium was replaced with fresh medium containing different concentrations of compound **3e** and incubated for another 10 days. Then, the cells were washed with PBS three times, fixed with 4% paraformaldehyde for 30 min and then stained with 0.1% Crystal violet stain. The plates were washed gently and then observed under a fluorescence microscope (Leica Inc., Germany). The percentage of colonies = number of treatment colonies/number of control colonies × 100%.

For the soft agar colony formation assay, A549 cells (1 × 10^5 cells/mL) were treated with different concentrations of compound **3e** in 1 mL of 0.3% RPMI-1640 medium-agar. The suspension was added on top of 2 mL of 0.6% RPMI-1640 medium-agar. The cultures were maintained at 37 °C and 5% CO_2 for 14 days, and the cell colonies were stained with 1.5 mg/mL NBT (nitrotetrazolium blue chloride). The next processing method was the same as that for the plate colony assay.

4.6. AO-EB and PI staining assay

A549 cells (3 × 10^5 cells/well) were seeded into 6-well plates in RPMI-1640 medium (Nest Biotechnology, China) and incubated for 12 h. Then, the medium was replaced with fresh medium containing different concentrations of compound **3e** and incubated for another 24 h.

For the AO-EB double staining assay, cells were washed twice with ice-cold PBS and stained with 100 μL of AO-EB stain (containing 1 mg/mL AO and 1 mg/mL EB in PBS) at room temperature for 10 min in the dark. Fluorescence was examined under a fluorescence microscope.

For the PI staining assay, A549 cells were harvested, centrifuged and washed twice with ice-cold PBS. The cells were stained with PI stain (50 mg/mL) at room temperature for 15 min in the dark. After centrifugation, the cells were washed twice with ice-cold PBS. The specimens were examined under a fluorescence microscope.

4.7. DNA fragmentation assay

The DNA cleavage pattern of A549 cells treated with compound **3e** was evaluated by observation of the formation of a DNA ladder[45] and according to the corresponding instructions of the genomic DNA isolation kit (TIANGEN, China). Briefly, A549 cells were treated with different concentrations of compound **3e** for 24 h, harvested and washed with ice-cold PBS. Then, the cells were lysed with DNA lysis buffer, treated with RNase A and digested with proteinase K. The DNA was precipitated using absolute ethanol, collected by centrifugation and subjected to 2% agarose gel electrophoresis for DNA fragmentation analysis.

4.8. Annexin V-FITC/PI double staining assay

A549 cells (3 × 10^5 cells/well) were seeded into 6-well plates (Nest Biotechnology, China) and incubated for 12 h. Then, the cells were treated with different concentrations of compound **3e** and incubated for another 24 h, harvested with trypsin and washed with ice-cold PBS. Finally, the collected cells were stained with Annexin V-FITC and PI according to the instructions of the Annexin V-FITC/PI apoptosis kit

(CoWin Biosciences, China). The samples were analysed by flow cytometry (BD Bioscience, USA).

4.9. Detection of reactive oxygen species (ROS) production

A549 cells (3×10^5 cells/well) were seeded into 6-well plates (Nest Biotechnology, China) and incubated for 12 h. Then, the cells were treated with different concentrations of compound **3e** and incubated for another 24 h, the medium was discarded and cells were washed with serum-free medium three times. Next, cells were stained with DCFH-DA (10 μM) (Beyotime Institute of Biotechnology, China) for 20 min at 37 °C in the dark. Finally, the fluorescence of the cells from each well was imaged with fluorescence microscope.

4.10. Caspase-3, -8 and -9 enzymatic activity assay

Caspase-3, -8 and -9 enzymatic activities were evaluated according to the corresponding instructions of the caspase colorimetric assay kits (KeyGEN BioTECH, USA). Briefly, 3×10^5 logarithmically growing A549 cells were seeded into each 6-well plate (Nest Biotechnology, China) and incubated for 12 h. The cells were treated with various concentrations of compound **3e** for 24 h, harvested with trypsin and washed with ice-cold PBS. Then, the collected cells were lysed on ice for 60 min. After centrifugation, the total protein concentration was measured using the BCA protein assay kit (Beyotime, China). Next, 5 μL of the corresponding caspase substrate was added to 50 μL of lysate containing 200 μg of protein and incubated at 37 °Cfor 4 h in the dark. The samples were measured at a wavelength of 405 nm using a microplate reader. According to the instructions of the caspase colorimetric assay kits, 50 μL PBS + 50 μL 2 × reaction was used as a blank control, and the corresponding degree of caspase activation = (induced group OD_{405} − blank group OD_{405}) / (control group OD_{405} − blank group OD_{405}).

4.11. Western blot assay

The A549 cells were treated with various concentrations of compound **3e** for 24 h, harvested and washed with cold PBS. Then, the collected cells were lysed in RIPA lysis buffer (Beyotime, China) containing 1 mM PMSF (Beyotime, China) on ice for 15 min. After centrifugation, the total protein concentration was measured using the BCA protein assay kit (Beyotime, China) and boiled with 5 × loading buffer for 5 min at 100 °C. Then, 20 μg of protein was separated on 8–12% SDS-PAGE and transferred to polyvinylidene difluoride (PVDF) membranes (Millipore, USA). The membranes were blocked with 5% skim milk at room temperature for 1 h and then incubated with primary antibodies overnight at 4 °C. The membranes were washed with TBST and incubated with anti-rabbit secondary antibodies for 1 h at room temperature. The immunoblots were observed with Clarity™ Western ECL Substrate (BIO-RAD, USA). Reagents and imaged using ChemiDoc™ Touch Imaging System (BIO-RAD, USA). Antibodies used were against MDM2 (#86934, Cell Signaling, USA), Cytochrome c (#11940, Cell Signaling, USA), Bcl-2 (#3498, Cell Signaling, USA), Bax (#2772, Cell Signaling, USA), Akt (#4691, Cell Signaling, USA), p21 (#2947, Cell Signaling, USA), β-actin (#4970, Cell Signaling, USA), HRP-linked anti-rabbit IgG (#7074, Cell Signaling, USA), 5-Lipoxygenase (ab39347, Abcam, USA) and p53 (ab131442, Abcam, USA).

4.12. Wound-healing assay

A549 cells were cultured in a 6-well plate (Nest Biotechnology, China) at 1×10^5 cells/per well until confluent monolayers formed. The monolayer of cells was scratched with a 10 μL sterile pipette tip. Then, the medium was replaced with fresh medium containing various concentrations of compound **3e** and incubated for another 36 h. The movement of cells was observed under the microscope. The migration area of the cells was calculated using the software provided with the microscope, and the percentage of migration in the control cells was taken as 100%.

4.13. Transwell assay

The cell migration and invasion assays were used to evaluate the colony migration ability of the compound **3e**-treated cells. Both experiments were slightly modified from previously reported methods.[46,47]

For the migration assay, A549 cells (1×10^4/mL) were suspended in RPMI-1640 medium containing 1% foetal bovine serum, and 100 μL of cell suspension was added to the upper chamber of each well of a 24-well transwell plate (Corning, USA). A total of 600 μL of RPMI-1640 medium containing 10% foetal bovine serum was added to the lower chamber. Then, the cells were treated with different concentrations of compound **3e** and incubated for 36 h. Each chamber was washed with PBS, fixed with methanol for 30 min and stained with 0.1% crystal violet for 20 min. A549 cells on the upper side of the membrane were removed with cotton swabs and photographed under a microscope. The cells that had migrated to the lower side of the membrane were counted, and the percentage of migration in the control cells was taken as 100%.

For the Matrigel-coated transwell assay, A549 cells (1×10^4/mL) were suspended in RPMI-1640 medium containing 1% foetal bovine serum, and 100 μL of cell suspension was seeded with Matrigel (Changsheng, Beijing, China) in each well of a 24-well transwell plate (Corning, USA). The remaining operations were the same as those for the migration assay.

4.14. Molecular docking studies

For preparation before docking, the structure of the target compound **3e** was obtained using ChemBioDraw Ultra 14.0 software and converted to 3D structure by ChemBio3D Ultra 14.0 software programs. The 3D structure of Akt (PDB ID: 3MV5), 5-Lox (PDB ID: 3V99) and MDM2 (PDB ID: 4ZYF) were downloaded from the Protein Data Bank, respectively, and then subjected to removal of water molecules and inhibitor treatment. Using Open Babel tool, the structure of the ligand and acceptor proteins were converted from a pdb file to a pdbqt file. After preparation, docking simulations were carried out using Autodock Vina.[48] The best-scoring poses as judged by the Vina docking score were selected, and used PyMOL software for visual analysis.

Acknowledgements

We are grateful for the financial support from the National Key R&D Program of China (2018YFC1708100), NSFC (81760625, 81660576 and 81560563), and Guizhou Projects (GNYL[2017]008 and QKHRC[2015]4032).

Appendix A. Supplementary data

Supplementary data to this article can be found online at https://doi.org/10.1016/j.bmc.2019.115109.

References

1. Viegas-Junior C, Danuello A, Bolzani VDS, Barreiro EJ, Fraga CAM. *Curr Med Chem.* 2007;14:1829–1852.
2. Fortin S, Bérubé G. *Expert Opin Drug Discov.* 2013;8:1029–1047.
3. Voskresensky ON, Levitsky AP. *Curr Med Chem.* 2002;2:691–714.
4. Li Y, Fang H, Xu W. *Mini Rev Med Chem.* 2007;7:663–678.
5. Wang HK. *Expert Opin Investig Drugs.* 2000;9:2103–2109.
6. Ren W, Qiao Z, Wang H, Zhang L. *Med Res Rev.* 2003;23:519–534.
7. Kelland LR. *Expert Opin Investig Drugs.* 2000;9:2903–2911.
8. Senderowicz AM, Sausville EA. *J Natl Cancer Inst.* 2000;92:376–387.
9. Fishkin RJ, Winslow JT. *Psychopharmacology.* 1997;132:335–341.

10. Habtemariam S. *J Nat Prod.* 1997;60:775–778.
11. Kubo I, Kinst Hori I, Choudhuri SK, Kubo Y, Sanchez Y, Ogura T. *Bioorg Med Chem.* 2000;8:1749–1755.
12. Liu YL, Ho DK, Cassady JM. *J Nat Prod.* 1992;55:357–363.
13. Pearce FL, Befs AD, Bienenstock J. *Allergy J Clin Immunol.* 1984;73:819–823.
14. Wolfman C, Viola H, Paladini A, Dajas F, Medina JH. *Pharmacol Biochem Behav.* 1994;47:1–4.
15. Peng CLV, Wang KR, Li QS, Chen J, Sun J, Zhu HL. *Bioorg Med Chem.* 2010;18:1117–1123.
16. Suresh Babu K, Hari Babu T, Srinivas PV, et al. *Bioorg Med Chem Lett.* 2006;16:221–224.
17. Xiao QZ, Sheng MP, Chang PH, Li FT, Han WD, Yuan JL. *Bioorg Med Chem Lett.* 2011;21:1222–1226.
18. Parmar VS, Jain SC, Bisht KS, et al. *Phytochemistry.* 1997;46:597–673.
19. Sun W, Cama LJ, Birzin ET, et al. *Bioorg Med Chem Lett.* 2006;16:1468–1472.
20. Stachulski AV, Berry NG, Low ACL, et al. *J Med Chem.* 2006;49:1450–1454.
21. Garino C, Bihel F, Pietrancosta N, et al. *Bioorg Med Chem Lett.* 2005;15:135–138.
22. Wang JL, Liu D, Zhang Z, et al. *Proc Natl Acad Sci U S A.* 2000;97:7124–7129.
23. Kemnitzer W, Kasibhatla S, Jiang S, et al. *Bioorg Med Chem Lett.* 2005;15:4745–4751.
24. Kemnitzer W, Drewe J, Jiang S, et al. *J Med Chem.* 2004;47:6299–6310.
25. Lotfy G, Said MM, El Ashry ESH, et al. *Bioorg Med Chem.* 2017;25:1514–1523.
26. Lotfy G, El Ashry ESH, Said MM, et al. *J Photochem Photobiol B Biol.* 2018;180:98–108.
27. Barakat A, Islam MS, Ghawas HM, et al. *RSC Adv.* 2018;8:14335.
28. Islam MS, Ghawas HM, El-Senduny FF, et al. *Bioorg Chem.* 2019;82:423–430.
29. Barakat, A.; Islam, M. S.; Al Majid, A. M.; Ghawas, H. M.; Badria, F. F.; Elshaier, Y. A. M. M.; Ghabbour, H. A. 2017, (US9822128B).
30. Mason JM, Lin DCC, Wei X, et al. *Cancer Cell.* 2014;26:163–176.
31. Wang S, Sun W, Zhao Y, et al. *Cancer Res.* 2014;74:5855–5865.
32. Yu B, Zheng YC, Shi XJ, Qi PP, Liu HM. *Anti Cancer Agents Med Chem.* 2016;16:1315–1324.
33. Han WY, Zhao JQ, Zuo J, Xu XY, Zhang XM, Yuan WC. *Adv Synth Catal.* 2015;357:3007–3031.
34. Mei G, Shi F. *Chem Commun.* 2018;54:6607–6621.
35. Cao ZY, Zhou F, Zhou J. *Acc Chem Res.* 2018;51:1443–1454.
36. CCDC1890559 contains the supplementary crystallographic datas for this paper. These data can be obtained free of charge from The Cambridge Crystallographic Data Centre via www.ccdc.cam.ac.uk/data_request/cif.
37. Zhang Y, Chen S, Wei C, Pankin GO, Ye X, Chen YC. *Eur J Med Chem.* 2018;147:218–226.
38. Mori S, Chang JT, Andrechek ER, et al. *Oncogene.* 2009;28:2796–2805.
39. Khwaja S, Fatima K, Hassanain M, et al. *Eur J Med Chem.* 2018;151:51–61.
40. Zhao TQ, Zhao YD, Liu XY, et al. *Eur J Med Chem.* 2018;151:327–338.
41. Yi JJ, Wang ZY, Bai HN, et al. *RSC Adv.* 2016;6:5278–5287.
42. Zhou MY, Ji SB, Wu ZJ, et al. *Eur J Med Chem.* 2018;96:92–97.
43. Huang RZ, Liang GB, Huang XC, et al. *Eur J Med Chem.* 2017;138:979–992.
44. Dyshlovoy SA, Fedorov SN, Kalinovsky AI, et al. *Marine Drugs.* 2012;10:1212–1224.
45. Li ZC, Xu XG, Huang Y, et al. *Int J Biol Sci.* 2012;8:394–405.
46. Ma LY, Zheng YC, Wang SQ, et al. *J Med Chem.* 2015;58:1705–1716.
47. Wang B, Zhao B, Pang LP, et al. *Pharm Res.* 2017;122:66–77.
48. Trott O, Olson AJ. *J Comput Chem.* 2010;31:445–461.